Energy spectrum of harmonically trapped two-component Fermi gases: Three- and four-particle problem

K. M. Daily and D. Blume

Department of Physics and Astronomy, Washington State University, Pullman, Washington 99164-2814, USA

Trapped two-component Fermi gases allow the investigation of the so-called BCS-BEC crossover by tuning the interspecies atom-atom s-wave scattering length $a^{(aa)}$ from attractive to repulsive, including vanishing and infinitely large values. Here, we numerically determine the energy spectrum of the equal-mass spin-balanced four-fermion system—the smallest few-particle system that exhibits BCS-BEC crossoverlike behavior—as a function of $a^{(aa)}$ using the stochastic variational approach. For comparative purposes, we also treat the two- and three-particle systems. States with vanishing and finite total angular momenta as well as with natural and unnatural parities are considered. In addition, the energy spectrum of weakly attractive and weakly repulsive gases is characterized by employing a perturbative framework that utilizes hyperspherical coordinates. The hyperspherical coordinate approach allows the straightforward assignment of quantum numbers and furthermore provides great insight into the strongly interacting unitary regime.

I. INTRODUCTION

Few-body systems show rich behaviors that range from the realization of highly correlated states to weakly bound Borromean states, and they have long been of great interest to chemists as well as nuclear and atomic physicists. To date, the determination of the entire energy spectrum, or parts thereof, of small bosonic or fermionic systems consisting of four or more constituents remains a challenge despite the ever increasing computational resources. Recently, significant progress has been made in the theoretical characterization of weakly bound bosonic tetramers [1–6]. In particular, for each Efimov trimer, there exist two tetramer states [4,5], which dissociate into four free bosons at critical negative scattering lengths. The ratio of the scattering length at which the trimer state becomes unbound and that at which the first or second tetramer state becomes unbound has been predicted to be universal [5]. Recently, this prediction has been confirmed by loss rate measurements on the negative scattering length side [7]. Working with an atomic Cs sample at temperatures just above the transition temperature to quantum degeneracy, the Innsbruck group [7] was able to observe enhanced losses at magnetic field strengths that correspond quite well to the theoretically predicted scattering length ratios [5]. By now, several groups have reported experimental evidence for universal four-boson physics [7–9].

While the universal properties of few-boson systems interacting through short-range potentials depend on two atomic physics parameters, i.e., the two-body s-wave scattering length $a^{(aa)}$ and a three-body parameter (see, e.g., Ref. [10]), the universal properties of dilute equal-mass two-component Fermi gases interacting through short-range potentials with interspecies s-wave interactions depend only on the s-wave scattering length [11–28]. Experimentally, small two-component Fermi gases can be realized by loading a deep three-dimensional optical lattice with a deterministic number of atoms per lattice site [29–31]. If the tunneling between neighboring sites is negligible, each lattice site can be treated as an independent, approximately harmonically confined few-fermion system.

This paper determines and characterizes the energy spectrum of three- and four-particle equal-mass two-component Fermi gases as a function of the s-wave scattering length under spherically symmetric harmonic confinement. For this confining geometry, the total angular momentum L_{tot} and the total parity Π_{tot} are good quantum numbers throughout the entire BCS-BEC crossover (BEC stands for Bose-Einstein condensate). The three-fermion spectra have been discussed previously [32–35] and are included here primarily for illustrative and comparative purposes. Our calculations follow two distinctly different avenues. On the one hand, we numerically determine the energy spectrum of few-fermion systems throughout the entire crossover. For the four-fermion system, we employ the stochastic variational approach [35–41]. In contrast to previous studies [35,40–43], we utilize basis functions with well-defined angular momentum and parity and determine the eigenenergies for a range of angular momenta. On the other hand, we determine the eigenspectrum semi-analytically within first-order degenerate perturbation theory. While necessarily limited to small $|a^{(aa)}|$, this approach allows the classification of a large portion of the energy spectrum in terms of appropriate quantum numbers. To characterize the energy spectrum in the weakly interacting regime, we employ hyperspherical coordinates [20,44–51] and write the noninteracting wave functions in the relative coordinates as a product of a hyperangular channel function and a hyperradial weight function. The eigenenergies of the noninteracting system have, in general, large degeneracies, which are partially lifted by the two-body interactions. The energy splittings can, to leading order, be calculated perturbatively. Compared to calculations that utilize Cartesian single-particle coordinates, one distinct advantage of the hyperspherical approach is that certain features carry over, with some modifications, to the strongly interacting unitary regime [20,35,42,50,52]. Our numerically determined spectra at unitarity can thus be interpreted within the hyperspherical framework.

The remainder of this manuscript is organized as follows. Section II A introduces the system Hamiltonian under study and provides other background information. Section II B

discusses the hyperspherical framework and its implications for the noninteracting, weakly interacting, and strongly interacting three- and four-fermion systems. The numerical basis set type expansion approaches for the three- and four-fermion problems are discussed in Secs. II C and II D, respectively. Section III summarizes our numerical and semianalytical perturbative results for the three- and four-fermion systems. We discuss the degeneracies and quantum numbers of the energy levels throughout the BCS-BEC crossover. Furthermore, we characterize the energy spectrum at unitarity and present a simple model that predicts the energy spectrum of the three-fermion system and a subset of the energy spectrum of the four-fermion system at unitarity. Lastly, Sec. IV summarizes our main results.

II. THEORETICAL BACKGROUND

This section introduces the system Hamiltonian and discusses our approaches to determining the eigenspectrum of equal-mass two-component Fermi gases perturbatively and numerically.

A. System Hamiltonian and other background information

We consider small equal-mass two-component Fermi gases under external harmonic confinement consisting of N atoms with mass m and position vectors $\vec{r}_j$, measured with respect to the center of the trap. Our model Hamiltonian H reads

$$H = H^{\mathrm{ni}} + V_{\mathrm{int}}(\vec{r}_1, \ldots, \vec{r}_N), \tag{1}$$

where the noninteracting Hamiltonian H^{ni} is given by

$$H^{\mathrm{ni}} = \sum_{j=1}^{N} \left[-\frac{\hbar^2}{2m} \nabla_{\vec{r}_j}^2 + V_{\mathrm{trap}}(\vec{r}_j) \right], \tag{2}$$

and the external spherically symmetric harmonic confining potential V_{trap} is characterized by the angular trapping frequency ω,

$$V_{\mathrm{trap}}(\vec{r}_j) = \tfrac{1}{2} m\omega^2 \vec{r}_j^2. \tag{3}$$

The potential V_{int} accounts for the short-range two-body interactions V_{tb} between unlike atoms,

$$V_{\mathrm{int}}(\vec{r}_1, \ldots, \vec{r}_N) = \sum_{j=1}^{N_\uparrow} \sum_{k=N_\uparrow+1}^{N} V_{\mathrm{tb}}(\vec{r}_j - \vec{r}_k), \tag{4}$$

where the number $N_\uparrow$ of spin-up atoms and the number $N_\downarrow$ of spin-down atoms add up to the total number of atoms, i.e., $N_\uparrow + N_\downarrow = N$. For spin-imbalanced systems, $N_\uparrow$ denotes the number of atoms of the majority species, and $N_\downarrow$ that of the minority species. Throughout, we assume that the two-body potential V_{tb} is characterized by the s-wave atom-atom scattering length $a^{(aa)}$ and possibly a range parameter r_0. The different functional forms of V_{tb} employed in our calculations are discussed below. The goal of this paper is to determine and interpret the eigenenergies $E(N_\uparrow, N_\downarrow)$ of the Hamiltonian H, Eq. (1).

If the atom-atom scattering length $a^{(aa)}$ is negative and small in absolute value, i.e., $|a^{(aa)}| \ll a_{\mathrm{ho}}$, where a_{ho} denotes the oscillator length associated with the atom mass m,

$$a_{\mathrm{ho}} = \sqrt{\frac{\hbar}{m\omega}}, \tag{5}$$

then the Fermi system behaves like a weakly attractive atomic gas. In this case, the energy shifts due to the interactions can be described, to leading order, within first-order degenerate perturbation theory that treats H^{ni} as the unperturbed Hamiltonian and V_{int} as the perturbation [35,41]. It is then convenient to parametrize the two-body potential $V_{\mathrm{tb}}(\vec{r}_{jk})$ by Fermi's pseudopotential $V_{\mathrm{F}}(\vec{r}_{jk})$ [53],

$$V_{\mathrm{F}}(\vec{r}_{jk}) = \frac{4\pi\hbar^2}{m} a^{(aa)} \delta(\vec{r}_{jk}), \tag{6}$$

which allows an analytical evaluation of the matrix elements and, if employed within first-order perturbation theory, does not lead to divergencies. In general, multiple eigenfunctions ψ_j^{ni} of the noninteracting atomic system are degenerate, and the first-order energy shifts $E^{(1)}$ are obtained by solving the determinantal equation

$$\det(\underline{V}_{\mathrm{int}} - E^{(1)}\underline{I}) = 0, \tag{7}$$

where $\underline{I}$ denotes the identity matrix and the matrix elements $(\underline{V}_{\mathrm{int}})_{jk}$ are given by

$$(\underline{V}_{\mathrm{int}})_{jk} = \langle \psi_j^{\mathrm{ni}} | V_{\mathrm{int}} | \psi_k^{\mathrm{ni}} \rangle. \tag{8}$$

Here, j and k run from 1 to g_{ni}, where g_{ni} denotes the degeneracy of the eigenenergy $E_{\mathrm{ni}}(N_\uparrow, N_\downarrow)$ under consideration.

The possibly most direct approach for constructing the eigenfunctions ψ_j^{ni} is to write the ψ_j^{ni} as a product of two determinants, one for the spin-up atoms and one for the spin-down atoms. The determinants themselves are constructed from the single-particle wave functions $\phi_{n_p,l_p,m_p}^{\mathrm{SP}}(\vec{r}_p)$, $p = 1, \ldots, N_\uparrow$ or $p = N_\uparrow + 1, \ldots, N$, which are eigenfunctions of the single-particle harmonic oscillator Hamiltonian H_p^{SP},

$$H_p^{\mathrm{SP}} = -\frac{\hbar^2}{2m} \nabla_{\vec{r}_p}^2 + V_{\mathrm{trap}}(\vec{r}_p). \tag{9}$$

Above, n_p, l_p, and m_p denote the single particle radial, orbital angular momentum and projection quantum numbers, respectively. For a given energy $E_{\mathrm{ni}}(N_\uparrow, N_\downarrow)$ of the noninteracting many-body system, the single-particle wave functions $\phi_{n_p,l_p,m_p}^{\mathrm{SP}}(\vec{r}_p)$ have to be chosen such that their eigenenergies obey the constraint

$$E_{\mathrm{ni}}(N_\uparrow, N_\downarrow) = \sum_{p=1}^{N_\uparrow} \left(2n_p + l_p + \frac{3}{2} \right) \hbar\omega$$
$$+ \sum_{p=N_\uparrow+1}^{N} \left(2n_p + l_p + \frac{3}{2} \right) \hbar\omega, \tag{10}$$

with the additional restriction that the sets of quantum numbers (n_p, l_p, m_p) and (n_q, l_q, m_q) differ by at least one entry for $p \neq q$, where $p, q = 1, \ldots, N_\uparrow$ or $p, q = N_\uparrow + 1, \ldots, N$. Following this approach, the first-order energy shifts $E^{(1)}$ of the energetically lowest-lying gaslike state for systems

with $N_\uparrow - N_\downarrow = 0, \pm 1$ and up to $N = 20$ atoms have been calculated [35].

Although in principle straightforward, the outlined construction of the wave functions of the noninteracting Fermi gas and their use in evaluating the energy shifts $E^{(1)}$ has several disadvantages. The number of degenerate states of the noninteracting system increases rapidly with increasing energy. For example, for the three-particle system with $(N_\uparrow, N_\downarrow) = (2,1)$, the lowest four energies $E_{\text{ni}}(2,1) = 11\hbar\omega/2, 13\hbar\omega/2, 15\hbar\omega/2$, and $17\hbar\omega/2$ of the noninteracting system have degeneracies $g_{\text{ni}} = 3, 18, 73$, and 228, and the determination of the energy shifts thus requires the construction and diagonalization of increasingly large interaction potential matrices $\underline{V}_{\text{int}}$. Furthermore, the outlined construction includes center-of-mass excitations and does not take advantage of the fact that the total angular momentum L_{tot}, the corresponding z-projection, and the parity Π_{tot} of the system are good quantum numbers. Lastly, the antisymmetrization is accomplished through the use of determinants, leading to $N_\uparrow! \times N_\downarrow!$ terms for each ψ_j^{ni}.

This paper pursues an alternative approach and writes the noninteracting wave functions in terms of hyperspherical coordinates [20,44–51]. This approach separates off the center-of-mass degrees of freedom, treats one angular momentum at a time, and ensures the proper antisymmetry of the wave function by utilizing angular momentum algebra. Using the wave functions of the noninteracting atomic Fermi gas, written in terms of hyperspherical coordinates, we are able to semianalytically determine the first-order energy shifts for a large portion of the spectrum of weakly interacting equal-mass two-component atomic Fermi gases with $N = 3$ and 4 (see Secs. II B and III).

When $a^{(aa)}$ is positive and small ($a^{(aa)} \ll a_{\text{ho}}$), diatomic bosonic molecules can form, and, if this happens, the Fermi system behaves like a weakly repulsive molecular Bose gas. In this limit, the dimers or diatomic molecules can, to a good approximation, be treated as bosonic point particles with mass $2m$ [16,35,41,54,55] and internal energy E_{dimer}; as detailed below, this internal energy accounts for the presence of the external confinement. The effective model systems for $N = 3$ and $N = 4$ then consist of two particles: an atom and a dimer in the three-particle case and two dimers in the four-particle case [35,41,54–56]. Separating off the center-of-mass motion, the dynamics are governed by the relative effective Hamiltonian H^{eff},

$$H^{\text{eff}} = -\frac{\hbar^2}{2\mu^{(k)}}\nabla_{\vec{r}}^2 + \frac{1}{2}\mu^{(k)}\omega^2\vec{r}^2 + V_{\text{F,reg}}^{(k)}(\vec{r}), \qquad (11)$$

where k stands for ad (atom-dimer) and dd (dimer-dimer) for the three- and four-fermion systems, respectively, and the position vector $\vec{r}$ denotes the atom-dimer and dimer-dimer distance vector for the three- and four-fermion systems, respectively. The reduced masses $\mu^{(ad)}$ and $\mu^{(dd)}$ of the atom-dimer and dimer-dimer systems are defined as $\mu^{(ad)} = 2m/3$ and $\mu^{(dd)} = m$. In this model, the atom-molecule and molecule-molecule interactions are conveniently described through Fermi's regularized pseudopotential $V_{\text{F,reg}}^{(k)}(\vec{r})$ [57],

$$V_{\text{F,reg}}^{(k)}(\vec{r}) = \frac{2\pi\hbar^2}{\mu^{(k)}}a^{(k)}\delta(\vec{r})\frac{\partial}{\partial r}r, \qquad (12)$$

with effective atom-dimer and dimer-dimer scattering lengths $a^{(ad)}$ and $a^{(dd)}$, respectively [23,35,56,58–60],

$$a^{(ad)} \approx 1.179\,066\,234\,9\,a^{(aa)} \qquad (13)$$

and [35,41,54]

$$a^{(dd)} \approx 0.608\,a^{(aa)}. \qquad (14)$$

The s-wave ($l_{\text{eff}} = 0$) eigenenergies E_{eff} of H^{eff} are readily obtained by solving the transcendental equation [61]

$$\frac{a^{(k)}}{a_{\text{ho},\mu}^{(k)}} = \frac{\Gamma\left(-\frac{E_{\text{eff}}}{2\hbar\omega} + \frac{1}{4}\right)}{2\Gamma\left(-\frac{E_{\text{eff}}}{2\hbar\omega} + \frac{3}{4}\right)}, \qquad (15)$$

where

$$a_{\text{ho},\mu}^{(k)} = \sqrt{\frac{\hbar}{\mu^{(k)}\omega}}. \qquad (16)$$

Since Fermi's regularized zero-range potential $V_{\text{F,reg}}^{(k)}$ only acts at $r = 0$, the eigenstates of H^{eff} with nonvanishing angular momentum l_{eff} do not feel the interaction, and the corresponding eigenenergies coincide with those of the noninteracting system. Figure 1 shows the relative eigenenergies $E_{\text{rel}}(1,1)$ obtained by solving Eq. (15) for $k = aa$ as a function of $a_{\text{ho}}/a^{(aa)}$ [in this case, $E_{\text{eff}} = E_{\text{rel}}(1,1)$ and $\mu^{(k)} = m/2$]. From Eq. (15) one finds at unitarity $E_{\text{unit,rel}}(1,1) = (2n_{\text{eff}} + 1/2)\hbar\omega$ for s-wave states. The eigenenergies E_{eff} of the effective atom-dimer and dimer-dimer systems can be obtained from Fig. 1 by appropriately scaling the horizontal axis.

Within the effective two-particle model, the relative energies $E_{\text{rel}}(2,1)$ and $E_{\text{rel}}(2,2)$ of the three- and four-fermion systems are given by $E_{\text{rel}}(2,1) = E_{\text{eff}} + E_{\text{dimer}}$ and $E_{\text{rel}}(2,2) = E_{\text{eff}} + 2E_{\text{dimer}}$, where the second terms on the right-hand sides account for the internal molecular binding energy of the dimer(s) in the presence of the trap [35,41]. E_{dimer} is given by the lowest energy solution of Eq. (15) with $k = aa$ and $\mu^{(aa)} = m/2$ (see solid line in Fig. 1). For $a^{(aa)} \ll a_{\text{ho}}$, the size of the dimer—given to first order by $a^{(aa)}$—is much smaller than the trap size, and E_{dimer} approaches the free-space result $E_{\text{dimer}}^{\text{free}} = -\hbar^2/[m(a^{(aa)})^2]$. As $a^{(aa)}$ increases, the role of the confinement becomes increasingly more important, and the lowest energy solution of Eq. (15) starts to deviate from $E_{\text{dimer}}^{\text{free}}$. Expanding Eq. (15) about the noninteracting energies
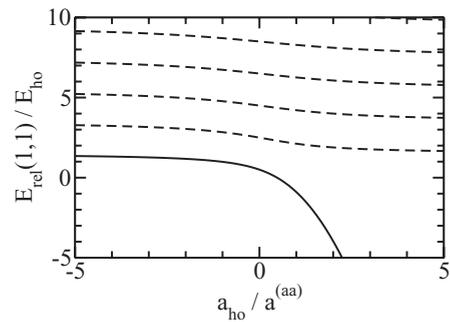
FIG. 1. Relative s-wave energies $E_{\text{rel}}(1,1)$ of the trapped atom-atom system, obtained by solving Eq. (15) for $k = aa$, as a function of $a_{\text{ho}}/a^{(aa)}$. The lowest s-wave eigenenergy (solid line) is referred to as E_{dimer} in the text. Here, E_{ho} denotes the harmonic oscillator energy, $E_{\text{ho}} = \hbar\omega$.

$(2n_{\text{eff}} + 3/2)\hbar\omega$, the s-wave energies E_{eff} can be approximated as [61]

$$E_{\text{eff}} \approx \left(2n_{\text{eff}} + 3/2 + \frac{2\Gamma(n_{\text{eff}} + 3/2)}{\sqrt{\pi}\,\Gamma(n_{\text{eff}} + 1)\Gamma(3/2)} \frac{a^{(k)}}{a_{\text{ho},\mu}^{(k)}}\right)\hbar\omega \tag{17}$$

for small $|a^{(k)}|$. Alternatively, this result can be obtained by treating the atom-dimer and dimer-dimer interactions within first-order perturbation theory.

Lastly, we discuss the angular momentum L_{rel} of the three- and four-fermion systems implied by the effective model Hamiltonian H^{eff}. If E_{eff} is taken to be one of the positive energy solutions of Eq. (15), then the total relative angular momentum L_{rel} of the three- and four-fermion systems is 0 and the states have natural parity, i.e., $\Pi_{\text{rel}} = +1$. If E_{eff} is taken to be an eigenenergy of H^{eff} with finite angular momentum l_{eff}, i.e., $E_{\text{eff}} = (2n_{\text{eff}} + l_{\text{eff}} + 3/2)\hbar\omega$ with $n_{\text{eff}} = 0, 1, \ldots$, then the total relative angular momentum of the three- and four-fermion systems is $L_{\text{rel}} = l_{\text{eff}}$ and the states have, as above, natural parity, i.e., $\Pi_{\text{rel}} = (-1)^{L_{\text{rel}}}$. These observations are used below to interpret Figs. 5 and 10.

B. Hyperspherical coordinate approach

The hyperspherical framework serves two distinct purposes in this paper. It allows (i) the construction of noninteracting wave functions with good quantum numbers and (ii) the classification of the energy spectrum at unitarity. This section first treats the noninteracting Fermi gas using hyperspherical coordinates and then reviews how the formalism, with some modifications, carries over to the infinitely strongly interacting unitary Fermi gas.

To construct the eigenfunctions of the noninteracting Fermi gas, we write the many-body Hamiltonian H^{ni}, Eq. (2), in hyperspherical coordinates [20,44–51]. We first separate off the center-of-mass vector $\vec{R}_{\text{c.m.}}$ and then divide the remaining $3N - 3$ coordinates into $3N - 4$ hyperangles, collectively denoted by $\vec{\Omega}$ (see below for their definition), and the hyperradius R,

$$R^2 = \frac{1}{N}\sum_{j=1}^{N}(\vec{r}_j - \vec{R}_{\text{c.m.}})^2. \tag{18}$$

Using these coordinates, the Hamiltonian H^{ni} can be written as

$$H^{\text{ni}} = H^{\text{c.m.}} - \frac{\hbar^2}{2M}\left(\frac{\partial^2}{\partial R^2} + \frac{3N - 4}{R}\frac{\partial}{\partial R}\right) + \frac{\Lambda^2}{2MR^2} + \frac{1}{2}M\omega^2 R^2, \tag{19}$$

where the center-of-mass Hamiltonian $H^{\text{c.m.}}$ is given by

$$H^{\text{c.m.}} = \frac{-\hbar^2}{2M}\nabla_{\vec{R}_{\text{c.m.}}}^2 + \frac{1}{2}M\omega^2 R_{\text{c.m.}}^2, \tag{20}$$

and M denotes the total mass of the system, i.e., $M = Nm$. In Eq. (19), Λ denotes the so-called grand angular momentum operator [44] that accounts for the kinetic energy associated

with the hyperangles $\vec{\Omega}$. The eigenfunctions ψ^{ni} of the Hamiltonian H^{ni} separate (see, e.g., Refs. [20,44,50]),

$$\psi^{\text{ni}}(\vec{r}_1, \ldots, \vec{r}_N) = G_{N_{\text{c.m.}}, L_{\text{c.m.}}, M_{\text{c.m.}}}(\vec{R}_{\text{c.m.}})F_{q,\lambda}(R)\Phi_{\lambda,\chi}(\vec{\Omega}). \tag{21}$$

Here, the center-of-mass functions $G_{N_{\text{c.m.}}, L_{\text{c.m.}}, M_{\text{c.m.}}}(\vec{R}_{\text{c.m.}})$ are eigenfunctions of $H^{\text{c.m.}}$, i.e., three-dimensional harmonic oscillator functions in the center-of-mass vector $\vec{R}_{\text{c.m.}}$, with eigenenergies $E_{\text{c.m.}} = (2N_{\text{c.m.}} + L_{\text{c.m.}} + 3/2)\hbar\omega$, where $N_{\text{c.m.}} = 0, 1, \ldots,$ $L_{\text{c.m.}} = 0, 1, \ldots,$ and $M_{\text{c.m.}} = -L_{\text{c.m.}}, -L_{\text{c.m.}} + 1, \ldots, L_{\text{c.m.}}$. The hyperspherical harmonics $\Phi_{\lambda,\chi}(\vec{\Omega})$, or so-called channel functions, are eigenfunctions of the operator Λ^2 [44],

$$\Lambda^2 \Phi_{\lambda,\chi}(\vec{\Omega}) = \hbar^2 \lambda(\lambda + 3N - 5)\Phi_{\lambda,\chi}(\vec{\Omega}), \tag{22}$$

where λ can take the values $0, 1, 2, \ldots$. The quantum number χ denotes the degeneracy for each λ [44],

$$\chi = \frac{(3N + 2\lambda - 5)(3N + \lambda - 6)!}{\lambda!(3N - 5)}. \tag{23}$$

In deriving Eq. (23), no symmetry constraints have been enforced. Below, we discuss the construction of the hyperspherical harmonics and the reduction of the degeneracy χ due to symmetry constraints for the three- and four-fermion systems. Since the center-of-mass coordinates and the hyperradius are unchanged under the exchange of $\vec{r}_j$ and $\vec{r}_k$ $(j, k = 1, \ldots, N)$, the symmetry constraints affect only the $\Phi_{\lambda,\chi}(\vec{\Omega})$ and neither $G_{N_{\text{c.m.}}, L_{\text{c.m.}}, M_{\text{c.m.}}}(\vec{R}_{\text{c.m.}})$ nor $F_{q,\lambda}(R)$.

Plugging Eq. (21) into the Schrödinger equation $H^{\text{ni}}\psi^{\text{ni}} = E_{\text{ni}}(N_{\uparrow}, N_{\downarrow})\psi^{\text{ni}}$ and dividing out the center-of-mass and hyperangular contributions, we obtain an effective hyperradial Schrödinger equation [20,50]

$$\left(-\frac{\hbar^2}{2M}\frac{\partial^2}{\partial R^2} + \frac{\hbar^2 K_{\text{ni}}(K_{\text{ni}} + 1)}{2MR^2} + \frac{1}{2}M\omega^2 R^2\right)\bar{F}_{q,\lambda}(R) = [E_{\text{ni}}(N_{\uparrow}, N_{\downarrow}) - E_{\text{c.m.}}]\bar{F}_{q,\lambda}(R), \tag{24}$$

where

$$\bar{F}_{q,\lambda}(R) = R^{(3N-4)/2}F_{q,\lambda}(R), \tag{25}$$

and

$$K_{\text{ni}} = \lambda + \frac{3N - 6}{2}. \tag{26}$$

Noticing that the effective hyperradial Schrödinger equation, Eq. (24), is formally identical to the Schrödinger equation for the three-dimensional harmonic oscillator with angular momentum K_{ni} [20,50], the eigenenergies $E_{\text{ni,rel}}$, $E_{\text{ni,rel}}(N_{\uparrow}, N_{\downarrow}) = E_{\text{ni}}(N_{\uparrow}, N_{\downarrow}) - E_{\text{c.m.}}$, and the corresponding eigenfunctions $\bar{F}_{q,\lambda}(R)$ are readily written down,

$$E_{\text{ni,rel}} = \left(2q + K_{\text{ni}} + \tfrac{3}{2}\right)\hbar\omega \tag{27}$$

with $q = 0, 1, \ldots,$ and

$$\bar{F}_{q,\lambda}(R) = N_{qK_{\text{ni}}} R^{K_{\text{ni}}+1} \exp\left(-\frac{R^2}{2a_M^2}\right) L_q^{(K_{\text{ni}}+1/2)}\left(\frac{R^2}{a_M^2}\right). \tag{28}$$

The normalization constant $N_{qK_{ni}}$ is chosen such that

$$\int_0^\infty |\bar{F}_{q,\lambda}(R)|^2 dR = 1, \qquad (29)$$

leading to

$$N_{qK_{ni}} = \sqrt{\frac{2^{K_{ni}+2}}{(2K_{ni}+1)!!\sqrt{\pi}L_q^{(K_{ni}+1/2)}(0)a_{ho,M}^{2K_{ni}+3}}}, \qquad (30)$$

where $L_q^{(K_{ni}+1/2)}$ denotes the associated Laguerre polynomial. The harmonic oscillator length $a_{ho,M} = \sqrt{\hbar/(M\omega)}$ can be interpreted as being associated with an effective mass M particle that moves along the hyperradial coordinate R. The quantity K_{ni} depends on λ and can be thought of as an effective angular momentum quantum number; it should be noted, though, that the K_{ni} are, in general, neither equal to the total angular momentum L_{tot} nor equal to the relative angular momentum L_{rel} of the two-component Fermi gas.

The explicit construction of the hyperspherical harmonics $\Phi_{\lambda,\chi}(\vec{\Omega})$ requires the hyperangles $\vec{\Omega}$ to be specified. The hyperangles $\vec{\Omega}$ can be defined in many different ways, and here we employ definitions that allow a straightforward antisymmetrization of the $\Phi_{\lambda,\chi}(\vec{\Omega})$. To this end, we introduce a set of mass scaled Jacobi vectors $\vec{u}_i$, $i = 1, \ldots, N - 1$, where [44,45]

$$\vec{u}_i = \sqrt{\frac{M}{\mu_i}}\vec{\rho}_i. \qquad (31)$$

Table I lists the Jacobi coordinates $\vec{\rho}_i$ and the associated reduced masses μ_i employed in this paper for the treatment of atomic two-component equal-mass three- and four-fermion systems. These Jacobi vectors have particularly convenient properties under the exchange of identical fermions. For the $(N_\uparrow, N_\downarrow) = (2,1)$ system, the Jacobi vector $\vec{\rho}_1$ changes sign under the exchange of the two spin-up fermions, while $\vec{\rho}_2$ remains unchanged. For the $(N_\uparrow, N_\downarrow) = (2,2)$ system, the exchange of the two spin-up fermions leads to a sign change of $\vec{\rho}_1$ while $\vec{\rho}_2$ and $\vec{\rho}_3$ remain unchanged, the exchange of the two spin-down fermions leads to a sign change of $\vec{\rho}_2$ while $\vec{\rho}_1$ and $\vec{\rho}_3$ remain unchanged, and the simultaneous exchange of the two spin-up fermions and the two spin-down fermions leads to a sign change of $\vec{\rho}_1$ and $\vec{\rho}_2$ while $\vec{\rho}_3$ remains unchanged. These properties of the Jacobi vectors make the construction of properly antisymmetrized hyperspherical harmonics $\Phi_{\lambda,\chi}(\vec{\Omega})$ for the three- and four-fermion systems comparatively simple. In terms of the mass-scaled Jacobi vectors $\vec{u}_i$, the $3N - 4$ hyperspherical angles $\vec{\Omega}$ are defined as $\vec{\Omega} = (\vec{u}_1/R, \ldots, \vec{u}_{N-1}/R)$ and the hyperradius R, Eq. (18), can be rewritten as $R^2 = \sum_{i=1}^{N-1} \vec{u}_i^2$ [44,45].

TABLE I. Definition of the Jacobi vectors $\vec{\rho}_i$ and the associated reduced masses μ_i used in our construction of the hyperspherical harmonics $\Phi_{\lambda,\chi}$ for the two-component equal-mass atomic Fermi gas with $(N_\uparrow, N_\downarrow) = (2,1)$ and $(2,2)$.

$(N_\uparrow, N_\downarrow)$	$\vec{\rho}_1$	$\vec{\rho}_2$	$\vec{\rho}_3$	μ_1	μ_2	μ_3
(2,1)	$\vec{r}_1 - \vec{r}_2$	$\frac{\vec{r}_1+\vec{r}_2}{2} - \vec{r}_3$		$\frac{m}{2}$	$\frac{2m}{3}$	
(2,2)	$\vec{r}_1 - \vec{r}_2$	$\vec{r}_3 - \vec{r}_4$	$\frac{\vec{r}_1+\vec{r}_2}{2} - \frac{\vec{r}_3+\vec{r}_4}{2}$	$\frac{m}{2}$	$\frac{m}{2}$	m

TABLE II. Characterization of the hyperspherical harmonics $\Phi_{\lambda,\chi}(\vec{\Omega})$ for the $(N_\uparrow, N_\downarrow) = (2,1)$ system with $\lambda \leqslant 5$. In determining χ, only hyperspherical harmonics that change sign under the exchange of the two spin-up atoms were counted.

λ	χ	K_{ni}	L_{rel}	Π_{rel}
1	3	5/2	1	−1
2	5	7/2	2	+1
2	3	7/2	1	+1
2	1	7/2	0	+1
3	14	9/2	3	−1
3	5	9/2	2	−1
3	6	9/2	1	−1
4	18	11/2	4	+1
4	14	11/2	3	+1
4	15	11/2	2	+1
4	3	11/2	1	+1
4	1	11/2	0	+1
5	33	13/2	5	−1
5	18	13/2	4	−1
5	28	13/2	3	−1
5	10	13/2	2	−1
5	9	13/2	1	−1

Following Avery [44], we construct a complete set of hyperspherical harmonics $\Phi_{\lambda,\chi}(\vec{\Omega})$, which are simultaneous eigenfunctions of the operators Λ^2, L_{rel}^2, $L_{rel,z}$, and Π_{rel}. Although the explicit functional forms of the $\Phi_{\lambda,\chi}(\vec{\Omega})$ are needed in our perturbative treatment, we restrict ourselves here to summarizing the degeneracies of the noninteracting eigenfunctions for the $(N_\uparrow, N_\downarrow) = (2,1)$ and $(2,2)$ systems (see Tables II and III).

Table II shows the degeneracies χ and quantum numbers of the hyperspherical harmonics for the $(N_\uparrow, N_\downarrow) = (2,1)$ system with λ up to 5; in constructing Table II, only hyperspherical harmonics that change sign under the exchange of the two spin-up atoms were counted. This symmetry constraint reduces the degeneracy of each λ manifold tremendously. Equation (23)—applicable to a system without symmetry constraints—gives 1, 6, 20, and 50 for $\lambda = 0, 1, 2,$ and 3, while Table II shows that the degeneracies are reduced to 0, 3, 9, and 25. Table II can be readily constructed by considering the angular momentum operators $\vec{l}_1$ and $\vec{l}_2$ associated with the Jacobi vectors $\vec{\rho}_1$ and $\vec{\rho}_2$, and by taking into account that $\vec{l}_1$ and $\vec{l}_2$ couple to $\vec{L}_{rel}$ [44]. Since $\vec{\rho}_1$ is the Jacobi vector that connects the two spin-up fermions, l_1 can only take odd values; l_2, in contrast, is not restricted by symmetry constraints, implying $l_2 = 0, 1, \ldots$. For a given λ, the allowed (l_1, l_2) combinations are determined by $\lambda = l_1 + l_2 + 2p$, where $p = 0, 1, \ldots$ [44,51]. Since the $(l_1, l_2) = (0,0)$ combination is symmetry-forbidden, the smallest allowed λ value is 1. For $\lambda = 1$, the only possible (l_1, l_2) combination is $(1,0)$, resulting in $L_{rel} = 1$, $\Pi_{rel} = (-1)^{l_1+l_2} = -1$, and a degeneracy of $\chi = 3$ (corresponding to three different projection quantum numbers M_L). For $\lambda = 2$, the only possible (l_1, l_2) combination is $(1,1)$, leading to $L_{rel} = 0, 1, 2,$ and $\Pi_{rel} = +1$. The degeneracy χ is 9 (1, 3, and 5 states for $L_{rel} = 0, 1,$ and 2, respectively). For $\lambda = 3$, the allowed (l_1, l_2) combinations are $(3,0)$, $(1,2)$, and

TABLE III. Characterization of the hyperspherical harmonics $\Phi_{\lambda,\chi}(\vec{\Omega})$ for the $(N_\uparrow, N_\downarrow) = (2,2)$ system with $\lambda \leqslant 5$. In determining χ, only hyperspherical harmonics that change sign under the exchange of the two spin-up atoms and the two spin-down atoms were counted.

λ	χ	K_{ni}	L_{rel}	Π_{rel}
2	5	5	2	+1
2	3	5	1	+1
2	1	5	0	+1
3	7	6	3	−1
3	10	6	2	−1
3	9	6	1	−1
3	1	6	0	−1
4	27	7	4	+1
4	28	7	3	+1
4	35	7	2	+1
4	12	7	1	+1
4	3	7	0	+1
5	33	8	5	−1
5	54	8	4	−1
5	77	8	3	−1
5	50	8	2	−1
5	27	8	1	−1
5	2	8	0	−1

TABLE IV. Coefficients $c^{(1)}$ for Fermi gas with $(N_\uparrow, N_\downarrow) = (2,1)$. The $c^{(1)}$ are defined through $E^{(1)} = c^{(1)}(2\pi)^{-1/2}\hbar\omega a^{(aa)}/a_{\mathrm{ho}}$.

$E_{\mathrm{ni,rel}}/(\hbar\omega)$	$g_{\mathrm{ni,rel}}$	L_{rel}	Π_{rel}	$c^{(1)}$
4	3	1	−1	3
5	5	2	+1	3/2
5	3	1	+1	0
5	1	0	+1	15/4
6	7	3	−1	9/4
6	7	3	−1	0
6	5	2	−1	0
6	3	1	−1	$\frac{3}{16}(13 + \sqrt{41})$
6	3	1	−1	$\frac{3}{16}(13 - \sqrt{41})$
6	3	1	−1	0

(1,0), leading to $L_{\mathrm{rel}} = 3$ (7 states), $L_{\mathrm{rel}} = 3,2,1$ (15 states), and $L_{\mathrm{rel}} = 1$ (3 states), respectively; thus, the degeneracy χ is 25. Following this reasoning, the remaining entries in Table II can be verified.

Table III summarizes the degeneracies and quantum numbers for the $(N_\uparrow, N_\downarrow) = (2,2)$ system. Similar to the three-fermion case, Table III is constructed by realizing that the angular momentum quantum numbers l_1 and l_2 associated with the Jacobi vectors $\vec{\rho}_1$ and $\vec{\rho}_2$ can only take odd values and that l_3, where l_3 denotes the angular momentum quantum number associated with the Jacobi vector $\vec{\rho}_3$, can take any value. For a given λ, the allowed (l_1, l_2, l_3) combinations are determined by $\lambda = l_1 + l_2 + l_3 + 2p + 2q$, where $p, q = 0, 1, \ldots$ [44,51]. Since both l_1 and l_2 have to be odd, the smallest allowed λ value is 2. In this case, $l_1 = l_2 = 1$ and $l_3 = 0$. The $\lambda = 2$ manifold thus consists of nine states [$\vec{l}_1$, $\vec{l}_2$, and $\vec{l}_3$ can couple so that $L_{\mathrm{rel}} = 2$ (5 states), 1 (3 states), and 0 (1 state)]. For $\lambda = 3$, the only possibility is $(l_1, l_2, l_3) = (1,1,1)$, implying 27 states. The angular momenta corresponding to these 27 states can be obtained by first coupling $\vec{l}_1$ and $\vec{l}_2$ to an intermediate angular momentum vector with quantum number 2, 1, or 0, and then coupling the intermediate angular momentum vector and $\vec{l}_3$ to obtain L_{rel}. The higher λ manifolds are treated following the same scheme.

Knowing the allowed λ and χ values, the degeneracy $g_{\mathrm{ni,rel}}$ of a given relative energy $E_{\mathrm{ni,rel}}(N_\uparrow, N_\downarrow)$ of the noninteracting trapped Fermi gas can be easily determined using Eqs. (26) and (27). These degeneracies are summarized in the second column of Tables IV and V for the three- and four-fermion systems, respectively. Alternatively [47,50], the relative energy $E_{\mathrm{ni,rel}}(N_\uparrow, N_\downarrow)$ of the noninteracting three- and four-fermion systems can be written as $E_{\mathrm{ni,rel}}(N_\uparrow, N_\downarrow) = \sum_{j=1}^{N-1}(2n_j + l_j + 3/2)\hbar\omega$, where $n_j = 0, 1, \ldots$ and where the allowed angular momentum quantum numbers l_j are determined by the symmetry requirements (see above). Counting the possible combinations of l_j and n_j values and taking the $(2l_j + 1)$ degeneracy associated with each l_j into account, gives the same results as those reported in the second column of Tables IV and V, and also allows—using Eqs. (26) and (27)—an independent determination of the λ and χ values given in the first two columns of Tables II and III.

So far, we have discussed the hyperspherical framework for the noninteracting two-component Fermi gas. We now review the modifications needed when applying this framework to the infinitely strongly interacting unitary gas with zero-range two-body interactions. The zero-range two-body potential with infinite $a^{(aa)}$ does not establish a meaningful length scale, leaving the oscillator length a_{ho} as the only length scale in the problem. Using scale invariance arguments, it has been shown [20] that a diverging s-wave scattering length $a^{(aa)}$ implies that the wave function $\psi^{\mathrm{unit}}(\vec{r}_1, \ldots, \vec{r}_N)$ at unitarity separates in the same way as that of the noninteracting system [see Eq. (21)]. It follows that Eq. (24) applies not only to the noninteracting gas but also to the unitary gas if K_{ni} is replaced by K_{unit} and if λ is reinterpreted as the eigenvalue of the hyperangular eigenequation that takes the two-body interactions into account. In the following, we use K_{unit} to denote the effective angular momentum of the unitary gas. Note that K_{unit} depends on the eigenvalue of the hyperangular eigenequation, i.e., there exists a K_{unit} for each channel function $\Phi_{\lambda,\chi}(\vec{\Omega})$; for notational convenience, we do not explicitly indicate the dependence of K_{unit} on the hyperangular quantum numbers.

The coefficients K_{unit} have been obtained for all states of the three-fermion system [32] (see also Refs. [62–64] for earlier work) and for the lowest 20 states with $(L_{\mathrm{rel}}, \Pi_{\mathrm{rel}}) = (0,+1)$ of the four-fermion system [65] by solving the hyperangular Schrödinger equation that includes the two-body interactions (see also Ref. [42]). The relative eigenenergies $E_{\mathrm{unit,rel}}$ of the unitary gas are, similar to the noninteracting case, given by [20]

$$E_{\mathrm{unit,rel}} = (2q + K_{\mathrm{unit}} + 3/2)\hbar\omega, \qquad (32)$$

and Eqs. (28)–(30) remain valid if K_{ni} is replaced by K_{unit} (and if λ is reinterpreted as discussed above). In Sec. III,

TABLE V. Coefficients $c^{(1)}$ for Fermi gas with $(N_\uparrow, N_\downarrow) = (2,2)$. The $c^{(1)}$ are defined through $E^{(1)} = c^{(1)}(2\pi)^{-1/2}\hbar\omega a^{(aa)}/a_{\mathrm{ho}}$.

$E_{\mathrm{ni,rel}}/(\hbar\omega)$	$g_{\mathrm{ni,rel}}$	L_{rel}	Π_{rel}	$c^{(1)}$
13/2	5	2	+1	5
13/2	3	1	+1	4
13/2	1	0	+1	13/2
15/2	7	3	−1	7/2
15/2	5	2	−1	3
15/2	5	2	−1	2
15/2	3	1	−1	5
15/2	3	1	−1	$\frac{1}{8}(29 + \sqrt{41})$
15/2	3	1	−1	$\frac{1}{8}(29 - \sqrt{41})$
15/2	1	0	−1	0
17/2	9	4	+1	$\frac{1}{8}(27 + \sqrt{73})$
17/2	9	4	+1	5/2
17/2	9	4	+1	$\frac{1}{8}(27 - \sqrt{73})$
17/2	7	3	+1	$\frac{1}{4}(9 + \sqrt{17})$
17/2	7	3	+1	3
17/2	7	3	+1	$\frac{1}{4}(9 - \sqrt{17})$
17/2	7	3	+1	0
17/2	5	2	+1	5.892 52
17/2	5	2	+1	5.310 30
17/2	5	2	+1	4.613 21
17/2	5	2	+1	3.217 83
17/2	5	2	+1	3.215 49
17/2	5	2	+1	1.921 29
17/2	5	2	+1	1.454 35
17/2	5	2	+1	0
17/2	3	1	+1	4.505 66
17/2	3	1	+1	3
17/2	3	1	+1	1.731 67
17/2	3	1	+1	0.5126 68
17/2	3	1	+1	0
17/2	1	0	+1	7.408 48
17/2	1	0	+1	6.981 38
17/2	1	0	+1	15/4
17/2	1	0	+1	2.891 39

we determine a number of K_{unit} coefficients by solving the full relative Schrödinger equation of the four-fermion system for various $L_{\mathrm{rel}} > 0$ and by then comparing the resulting energy with the right-hand side of Eq. (32). Lastly, we note that Eq. (32) implies that the excitation spectrum of the trapped unitary two-component Fermi gas contains ladders of excitation frequencies that are integer multiples of $2\hbar\omega$, independent of the actual values of K_{unit} [14,19,20].

C. Numerical treatment of the three-fermion system: Lippmann-Schwinger equation

The trapped three-fermion problem with zero-range interactions and arbitrary s-wave scattering length $a^{(aa)}$ has been solved using a number of different semianalytical and numerical approaches [33–35]. Here, we replace the regularized zero-range pseudopotential $V_{\mathrm{F,reg}}^{(aa)}(\vec{r})$, which describes the interactions between atoms with opposite spins, by the corresponding Bethe-Peierls boundary condition and employ an approach developed by Kestner and Duan [33] that is

based on the Lippmann-Schwinger equation. This approach reduces the three-body problem to solving a set of coupled equations [33],

$$\frac{2\Gamma(-\nu_j)}{\Gamma\left(-\nu_j - \frac{1}{2}\right)}c_j + \sum_{k=1}^{B} d_{jk}c_k = \left(\frac{a_{\mathrm{ho},\mu}^{(aa)}}{a^{(aa)}}\right)c_j, \quad (33)$$

for the eigenvector $\vec{c} = (c_1, \ldots, c_B)$ and the eigenvalue $(a^{(aa)}/a_{\mathrm{ho},\mu}^{(aa)})^{-1}$. In Eq. (33), the ν_j denote noninteger quantum numbers that depend on $E_{\mathrm{rel}}(2,1)$ and the d_{jk} dimensionless matrix elements. Their definitions are given in Refs. [33,66].

In the $B \to \infty$ limit, Eq. (33) gives the exact three-fermion energy spectrum. For each $E_{\mathrm{rel}}(2,1)$, there exist multiple $\vec{c}$ and $a^{(aa)}$ that solve Eq. (33). Thus, Eq. (33) can be interpreted as a matrix equation with eigenvector matrix $\underline{c} = (\vec{c}_1, \ldots, \vec{c}_B)$ and eigenvalue vector $((a^{(aa)})_1, \ldots, (a^{(aa)})_B)$. The solutions obtained by solving Eq. (33) belong to three-fermion states with natural parity. For the three-fermion system, unnatural parity states are not affected by the s-wave zero-range interactions and coincide with those of the noninteracting system. For each L_{rel}, we solve the matrix problem for different B, using $B \leqslant 50$. For positive $E_{\mathrm{rel}}(2,1)$, our results presented in Sec. III A are obtained using $B = 50$. For negative $E_{\mathrm{rel}}(2,1)$, we use somewhat smaller B values; we have checked through extrapolation to the $B \to \infty$ limit that the three-fermion energies obtained in this manner are highly accurate. We find, e.g., that the eigenenergies at unitarity obtained by the numerical approach based on the Lippmann-Schwinger equation [33] agree to better than 0.01% with those obtained by solving the transcendental equation derived by Werner and Castin [32].

D. Numerical treatment of the four-fermion system: Stochastic variational approach

To determine the energy spectrum of two-component Fermi gases with $(N_\uparrow, N_\downarrow) = (2,2)$ under spherically symmetric harmonic confinement, we employ the stochastic variational approach [35–41]. Our implementation separates off the center-of-mass degrees of freedom $\vec{R}_{\mathrm{c.m.}}$, defines a set of $N - 1$ Jacobi coordinates $\vec{x} = (\vec{\rho}_1, \ldots, \vec{\rho}_{N-1})$, and expands the relative wave function $\psi_{\mathrm{rel}}(\vec{x})$ in terms of the basis functions $\varphi_k(\vec{x})$,

$$\psi_{\mathrm{rel}}(\vec{x}) = \sum_{k=1}^{B} \mathcal{A}[c_k\varphi_k(\vec{x})], \quad (34)$$

where the antisymmetrization operator $\mathcal{A}$ can be written as $\mathcal{A} = 1 - P_{12} - P_{34} + P_{12}P_{34}$ for the $(N_\uparrow, N_\downarrow) = (2,2)$ system. In Eq. (34), the c_k denote expansion coefficients. We parametrize the two-body potential V_{tb} by a spherically symmetric attractive Gaussian with depth V_0 ($V_0 > 0$) and range r_0,

$$V_G(\vec{r}) = -V_0 \exp\left[-\left(\frac{r}{\sqrt{2}r_0}\right)^2\right]; \quad (35)$$

this interaction potential is convenient since the matrix elements $\langle\varphi_j|V_G|\varphi_k\rangle$ are—for the φ_k employed in this work— known analytically [38] (see below for the definition of the φ_k). For a given range r_0, we adjust the depth V_0 such that

V_G reproduces the desired s-wave scattering length $a^{(aa)}$. For negative (positive) $a^{(aa)}$, we restrict ourselves to parameter combinations for which $V_G(\vec{r})$ supports no (one) s-wave free-space bound state. For each $a^{(aa)}$, we consider a number of different ranges $r_0 \ll a_{ho}$, and extrapolate to the $r_0 \to 0$ limit (see Sec. III B for details).

We employ two different classes of nonorthogonal basis functions φ_k. For both classes, the Hamiltonian matrix elements and overlap matrix elements are known analytically [38], thus reducing the problem of finding the eigenenergies and eigenfunctions to diagonalizing a generalized eigenvalue problem. The first class of basis functions $\varphi_k(\vec{x})$ has well-defined angular momentum L_{rel} and natural parity, while the latter class has neither well-defined angular momentum L_{rel} nor well-defined parity Π_{rel}.

To describe natural parity states with well-defined angular momentum L_{rel} and corresponding projection quantum number M_L, we employ the following basis functions [38]:

$$\varphi_k(\vec{x}) = |\vec{v}^{(k)}|^{L_{rel}} Y_{L_{rel}M_L}(\hat{v}^{(k)}) \exp\left(-\tfrac{1}{2}\vec{x}^T \underline{A}^{(k)}\vec{x}\right), \quad (36)$$

where

$$\vec{v}^{(k)} = \sum_{j=1}^{N-1} u_j^{(k)} \vec{\rho}_j. \quad (37)$$

Here, the $u_j^{(k)}$, $j = 1, \ldots, N-1$, define a $(N-1)$-dimensional parameter vector that determines how the angular momentum L_{rel} is distributed among the $(N-1)$ Jacobi vectors $\vec{\rho}_j$. In Eq. (36), $\underline{A}^{(k)}$ denotes a $(N-1) \times (N-1)$-dimensional symmetric matrix, which is described by $N(N-1)/2$ independent parameters. To get a physical interpretation of these parameters, we rewrite the exponent on the right-hand side of Eq. (36) in terms of a sum over the square of interparticle distances r_{ij} and $N(N-1)/2$ widths $d_{ij}^{(k)}$,

$$\frac{1}{2}\vec{x}^T \underline{A}^{(k)}\vec{x} = \frac{1}{2}\sum_{i=1}^{N-1}\sum_{j=1}^{N-1} A_{ij}^{(k)} \vec{\rho}_i \cdot \vec{\rho}_j = \sum_{i<j}^{N}\left(\frac{r_{ij}}{\sqrt{2}d_{ij}^{(k)}}\right)^2. \quad (38)$$

The explicit relationship between the parameter matrix $\underline{A}^{(k)}$ and the widths $d_{ij}^{(k)}$ ($i < j$) can be determined by expressing the interparticle distance vectors $\vec{r}_{ij}$ in terms of the Jacobi vectors $\vec{x}$ [38]. Equation (38) illustrates that the $d_{ij}^{(k)}$ determine the widths of Gaussian functions in the interparticle distance coordinates. In our calculations, we choose a set of widths $d_{ij}^{(k)}$ for each basis function and construct the matrix $\underline{A}^{(k)}$ from these. The widths $d_{ij}^{(k)}$ themselves are—guided by physical arguments—determined semistochastically following the schemes discussed in Refs. [35,38,40]. For the $(N_\uparrow, N_\downarrow) = (2,2)$ system with small r_0 and small positive $a^{(aa)}$, e.g., three- and four-body bound states are absent [54,56], implying that at most two of the widths $d_{13}^{(k)}$, $d_{14}^{(k)}$, $d_{23}^{(k)}$, and $d_{24}^{(k)}$ (but not $d_{13}^{(k)}$ and $d_{14}^{(k)}$ simultaneously or $d_{23}^{(k)}$ and $d_{24}^{(k)}$ simultaneously) should be of the order of the two-body range r_0 for a given k. We use the basis functions given in Eq. (36) to determine the eigenenergies of states with vanishing and finite L_{rel} and natural parity, i.e., $\Pi_{rel} = (-1)^{L_{rel}}$.

To describe states with unnatural parity, we employ basis functions φ_k that are neither eigenfunctions of the angular momentum operator L_{rel} nor the parity operator Π_{rel} [38],

$$\varphi_k(\vec{x}) = \exp\left(-\tfrac{1}{2}\vec{x}^T \underline{A}^{(k)}\vec{x} + (\vec{s}^{(k)})^T \vec{x}\right). \quad (39)$$

Here, the quantity $\vec{s}^{(k)}$ consists of $N-1$ three-dimensional parameter vectors, and $(\vec{s}^{(k)})^T \vec{x}$ is just the dot product between two $3(N-1)$-dimensional vectors. The $3(N-1)$ parameters of $\vec{s}^{(k)}$ are, together with the $N(N-1)/2$ parameters of the matrix $\underline{A}^{(k)}$, optimized semistochastically [38]. Since the basis functions defined in Eq. (39) are not eigenfunctions of L_{rel}, M_L, or Π_{rel}, their use allows the determination of the entire energy spectrum at once. In Sec. III B, we employ the basis functions given in Eq. (39) to determine the energetically lowest-lying unnatural parity state of the four-fermion system with negative $a^{(aa)}$.

Following the schemes outlined, the determination of the four-fermion energies corresponding to unnatural parity states is significantly less numerically efficient than that of natural parity states. This is, of course, not surprising since only a "fraction" of the basis functions given in Eq. (39) contributes to describing states with the desired angular momentum, projection quantum number, and parity.

III. RESULTS

This section summarizes the energetics of the three- and four-particle equal-mass Fermi gas.

A. Three-fermion system

Figures 2(a) and 2(b) show the eigenenergies $E_{rel}(2,1)$ for states with natural parity and $L_{rel} = 0$ and 1 as a function of the inverse scattering length $1/a^{(aa)}$. The symbols show the solutions to the coupled equations, Eq. (33), while the solid and dashed lines are obtained from our perturbative treatments of the atomic Fermi gas and the effective atom plus dimer model, respectively. Note that the perturbative treatment of the atomic Fermi gas (solid lines) describes the energy levels corresponding to gaslike states for negative as well as positive $a^{(aa)}$ ($|a^{(aa)}|$ small). In the following, we highlight selected characteristics of the three-fermion energy spectrum.

We first consider the weakly interacting attractive Fermi gas. In the noninteracting limit, $a^{(aa)} \to 0^-$, the ground state has an energy of $E_{ni,rel} = 4\hbar\omega$ and is characterized by $L_{rel} = 1$ and $\Pi_{rel} = -1$ (see Fig. 2 and Table IV). For the next family of energies with $E_{ni,rel} = 5\hbar\omega$, we have two natural parity states with $L_{rel} = 0$ and $L_{rel} = 2$, and one unnatural parity state with $L_{rel} = 1$. The fact that the lowest noninteracting $L_{rel} = 0$ state has a higher energy than the lowest noninteracting $L_{rel} = 1$ state can be understood intuitively by realizing that the two like atoms cannot both occupy the lowest single-particle state. Within the hyperspherical description, this implies that the $L_{rel} = 0$ state with $\lambda = 0$ and $q = 0$ is symmetry-forbidden (see Sec. II B) and that the first symmetry-allowed $L_{rel} = 0$ state, which has $\lambda = 2$ and $q = 0$, lies $2\hbar\omega$ higher in energy than the symmetry-forbidden $L_{rel} = 0$ state.

The coefficients $c^{(1)}$ that determine the perturbative energy shifts $E^{(1)}$ of the atomic $(N_\uparrow, N_\downarrow) = (2,1)$ system are
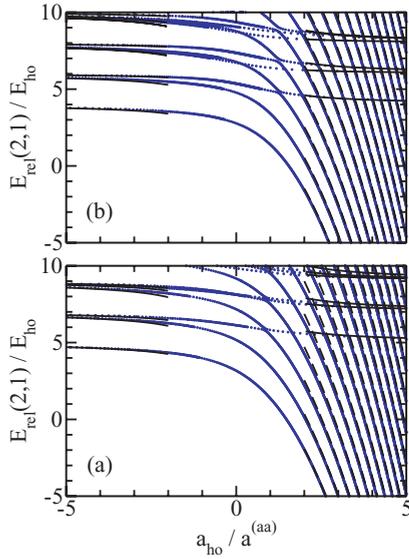
FIG. 2. (Color online) Three-fermion energies for (a) $(L_{rel}, \Pi_{rel}) = (0, +1)$ and (b) $(L_{rel}, \Pi_{rel}) = (1, -1)$ as a function of the inverse s-wave scattering length $a_{ho}/a^{(aa)}$. Symbols show the essentially exact zero-range energies obtained by solving Eq. (33). Solid lines show the energies obtained by treating the noninteracting atomic Fermi gas perturbatively for negative and positive $a^{(aa)}$, while dashed lines show the energies obtained by treating the effective atom plus dimer system perturbatively.

calculated semianalytically following the scheme outlined in Secs. II A and II B, and reported in the last column of Table IV for the first three energy families. As already mentioned, the unnatural parity states of the three-fermion system are unaffected by the interactions [20,33,66]. This behavior is specific to zero-range s-wave interactions, since a finite-range potential allows, in general, an energy shift due to p-wave or other higher partial-wave interactions. To illustrate the validity regime of the perturbative expressions, Figs. 3(a)–3(d) show the small $|a^{(aa)}|$ region, $a^{(aa)} \leqslant 0$, of the three-body energy spectrum as a function of $|a^{(aa)}|/a_{ho}$ for the energies around the first four energy families with $E_{rel}(2,1) \approx 4\hbar\omega$ to $E_{rel}(2,1) \approx 7\hbar\omega$. As in Fig. 2, the exact energies are shown by symbols, while the perturbative energies corresponding to natural parity states are shown by solid lines. As expected, the perturbative treatment reproduces the exact energies extremely well for small $|a^{(aa)}|/a_{ho}$ and provides a semiquantitatively correct description up to $|a^{(aa)}| \approx 0.5a_{ho}$ (see also Fig. 2, which shows the perturbative energies up to $a_{ho}/|a^{(aa)}| = 2$ or $|a^{(aa)}| = 0.5a_{ho}$).

Table IV shows that the coefficients $c^{(1)}$ cover a wide range of values. Within each energy family, the state shifted most strongly by the interactions is a natural parity state with the smallest allowed angular momentum L_{rel}. To illustrate the increasing density of states and the spread of the energy levels around the noninteracting degenerate energy manifold, Figs. 4(a) and 4(b) show the frequency with which the coefficients $c^{(1)}$ occur for $E_{rel}(2,1) \approx 7\hbar\omega$ (fourth energy manifold) and $E_{rel}(2,1) \approx 8\hbar\omega$ (fifth energy manifold), respectively. In making this plot, the $2L_{rel} + 1$ degeneracy of the energy levels has been taken into account. Since the unnatural parity states are not affected by the zero-range interactions, the
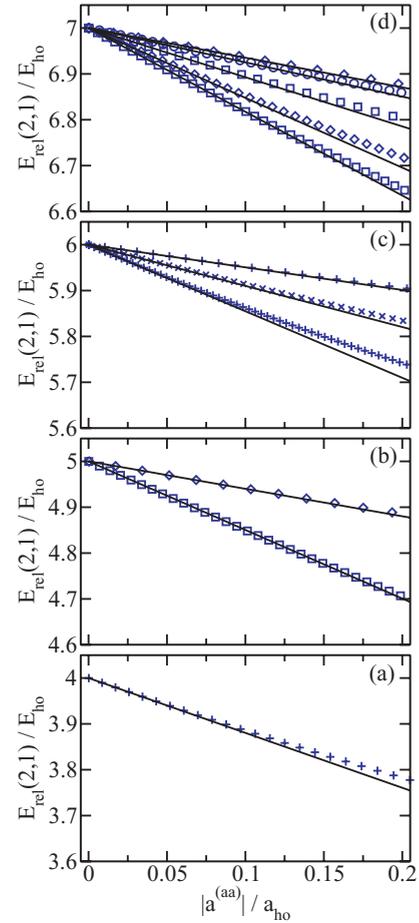
FIG. 3. (Color online) Three-fermion energies as a function of the absolute value of the s-wave scattering length $|a^{(aa)}|$ for small $|a^{(aa)}|$, $a^{(aa)} \leqslant 0$, and (a) $E_{rel}(2,1) \approx 4\hbar\omega$, (b) $E_{rel}(2,1) \approx 5\hbar\omega$, (c) $E_{rel}(2,1) \approx 6\hbar\omega$, and (d) $E_{rel}(2,1) \approx 7\hbar\omega$. Squares, pluses, diamonds, crosses, and circles show the essentially exact zero-range energies obtained by solving Eq. (33) for $L_{rel} = 0$–4. For comparison, solid lines show the perturbative results for natural parity states. The solid lines correspond to (a) $(L_{rel}, \Pi_{rel}) = (1, -1)$; and from bottom to top to (b) $(L_{rel}, \Pi_{rel}) = (0, +1)$ and $(2, +1)$; (c) $(L_{rel}, \Pi_{rel}) = (1, -1)$, $(3, -1)$, and $(1, -1)$; and (d) $(L_{rel}, \Pi_{rel}) = (0, +1)$, $(2, +1)$, $(0, +1)$, $(4, +1)$, and $(2, +1)$.

distribution of the $c^{(1)}$ coefficients shows a large amplitude for the $c^{(1)} = 0$ bin. Figures 4(a) and 4(b) show that the spread of the coefficients $c^{(1)}$ increases slightly as the energy manifold increases. The primary characteristic of the distributions of the $c^{(1)}$ coefficients is, however, that the amplitude increases with increasing energy.

We now consider the weakly repulsive regime, i.e., the regime where $a^{(aa)}/a_{ho} \ll 1$ and $a^{(aa)} > 0$. In this regime, Fig. 2 shows two families of energy levels: (i) energy levels with positive energy and (ii) those with negative energy. The positive energy branches correspond to states that describe a gas of atoms; we refer to these states as the "gaslike state" family. The energies of this family are, in the $a^{(aa)} \rightarrow 0^+$ limit, well described by treating the atomic Fermi gas perturbatively (see solid lines in Fig. 2). The negative energy branches correspond to states that can be thought of as consisting of
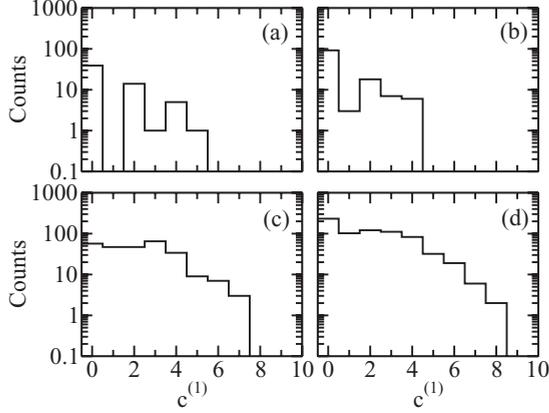
FIG. 4. Frequency of the coefficients $c^{(1)}$, which characterize the energy shifts $E^{(1)}$ of the weakly interacting atomic Fermi gas, for the three- and four-fermion systems. Panels (a) and (b) show the distribution of the $c^{(1)}$ coefficients for $E_{rel}(2,1) \approx 7\hbar\omega$ (fourth energy manifold of the three-fermion system) and for $E_{rel}(2,1) \approx 8\hbar\omega$ (fifth energy manifold of the three-fermion system). Panels (c) and (d) show the distribution of the $c^{(1)}$ coefficients for $E_{rel}(2,2) \approx 19\hbar\omega/2$ (fourth energy manifold of the four-fermion system) and for $E_{rel}(2,2) \approx 21\hbar\omega/2$ (fifth energy manifold of the four-fermion system). Note the log scale of the vertical axis.

a bound diatomic molecule and a spare atom; we refer to these states as "dimer plus atom" family. In agreement with the literature (see, e.g., Ref. [56]), Fig. 2 shows that the formation of bound triatomic molecules is prohibited by the Pauli exclusion principle or the so-called Pauli pressure. For small and positive $a^{(aa)}$, the perturbative energy shifts for the energy levels with $L_{rel} = 0$ and $\Pi_{rel} = +1$ [dashed lines in Fig. 2(a)] are calculated using Eq. (17) with $k = ad$. The perturbative approach, applied to the effective model Hamiltonian H^{eff}, predicts no energy shift for states with $L_{rel} > 0$. This follows directly from the fact that we parametrized the effective atom-dimer interaction through a zero-range s-wave potential. Thus, the "bending" of the dashed lines in Fig. 2(b) for $L_{rel} = 1$ (and in general, $L_{rel} > 0$) and positive $a^{(aa)}$ is solely due to the internal energy of the dimer and not due to the effective atom-dimer interaction. We find that the perturbative treatment provides a qualitatively correct description up to $a^{(aa)} \approx 0.5a_{ho}$.

The effective model Hamiltonian H^{eff} also provides an intuitive picture for why the lowest $L_{rel} = 0$ state has a lower energy than the lowest $L_{rel} = 1$ state as $a^{(aa)} \to 0^+$. In the $a^{(aa)} \to 0^+$ limit, the diatomic molecule has vanishing angular momentum and the angular momentum L_{rel} must be carried by the atom-dimer distance vector. Thus, the energy of the lowest state with $L_{rel} = 1$ lies approximately $\hbar\omega$ above the lowest state with $L_{rel} = 0$, the energy of the lowest state with $L_{rel} = 2$ lies approximately $\hbar\omega$ above the lowest state with $L_{rel} = 1$, and so on. The parity inversion of the energetically lowest-lying state ($L_{rel} = 1$ and $\Pi_{rel} = -1$ in the $a^{(aa)} \to 0^-$ limit, and $L_{rel} = 0$ and $\Pi_{rel} = +1$ in the $a^{(aa)} \to 0^+$ limit) occurs at $a_{ho}/a^{(aa)} \approx 1$ and has already been pointed out in a number of works [33–35].

Motivated by the fact that the energy spectrum of the three-fermion system can be described by an effective atom plus
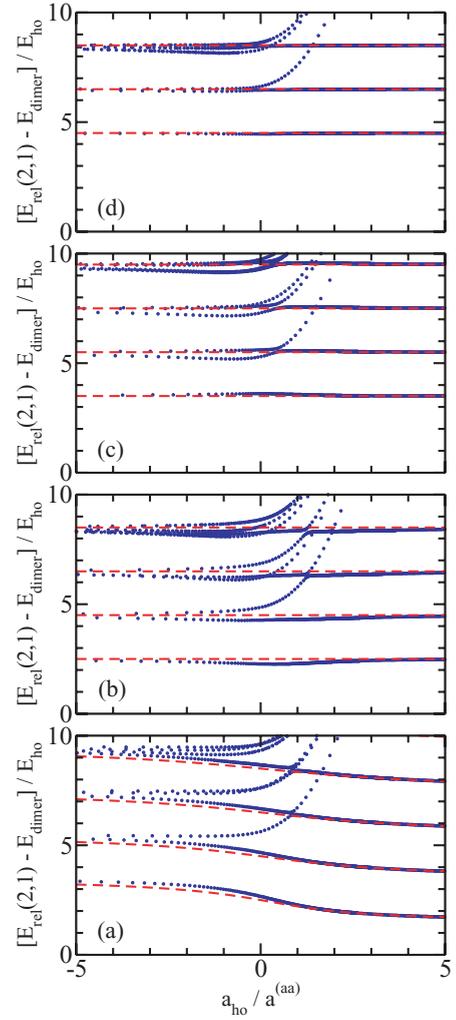
FIG. 5. (Color online) Symbols show the scaled energies $E_{rel}(2,1) - E_{dimer}$ as a function of the inverse scattering length $a_{ho}/a^{(aa)}$ for (a) $(L_{rel}, \Pi_{rel}) = (0,+1)$, (b) $(L_{rel}, \Pi_{rel}) = (1,-1)$, (c) $(L_{rel}, \Pi_{rel}) = (2,+1)$, and (d) $(L_{rel}, \Pi_{rel}) = (3,-1)$. For comparison, dashed lines show the energies predicted by the effective atom-dimer model, which provides a semiquantitative description of the states belonging to the "atom plus dimer" family (see text for details).

dimer model in the $a^{(aa)} \to 0^+$ limit, symbols in Figs. 5(a)–5(d) show the quantity $E_{rel}(2,1) - E_{dimer}$ as a function of the inverse atom-atom scattering length $1/a^{(aa)}$ for $L_{rel} = 0$–3. Here, E_{dimer} denotes the lowest eigenenergy of the trapped s-wave interacting atom-atom system, i.e., the lowest eigenenergy of Eq. (15) with $k = aa$. The quantity $E_{rel}(2,1) - E_{dimer}$ has been investigated previously [33,35] and has been termed the universal energy crossover curve in Ref. [35]. Figures 5(b)–5(d) show the existence of a family of states for $L_{rel} > 0$ whose scaled energies are nearly independent of the s-wave scattering length $a^{(aa)}$. These scaled energies are approximately given by $(2n_{eff} + L_{rel} + 3/2)\hbar\omega$ [see dashed lines in Figs. 5(b)–5(d)]. The fairly good agreement between the symbols and the dashed lines reflects the fact that a subset of the three-fermion energies can be described to a fairly good approximation by treating the three-fermion system as consisting of a bound trapped s-wave

dimer plus a noninteracting spare atom. Figures 5(b)–5(d) show that this effective dimer-atom description improves with increasing L_{rel}.

The fact that a subset of states of the three-particle spectrum is reasonably well described by the effective dimer plus atom model suggests that the three-particle energy spectrum can be described in terms of avoided crossings between "atom plus dimer" states and "gaslike" states. An interpretation along this line has been quantified by von Stecher [67] who applied a diabatization scheme. Here, we do not follow the diabatization scheme but instead offer a qualitative discussion of the natural parity three-fermion spectrum with $L_{rel} > 0$. We make four observations: (i) A sequence of states has an energy $E_{rel}(2,1)$ of approximately $(2 + L_{rel} + 2n)\hbar\omega$ at unitarity, an energy $E_{rel}(2,1)$ of approximately $(3 + L_{rel} + 2n)\hbar\omega$ in the $a^{(aa)} \to 0^-$ limit, and an energy $E_{rel}(2,1)$ of approximately $E_{dimer} + (3/2 + L_{rel} + 2n)\hbar\omega$ in the $a^{(aa)} \to 0^+$ limit [see Fig. 2(b); the states discussed here are those with approximately constant $E_{rel}(2,1) - E_{dimer}$, see Figs. 5(b)–5(d)]. (ii) For each L_{rel}, the degeneracy of the energy families with $E_{ni,rel} = (3 + L_{rel} + 2n)\hbar\omega$, $n = 0, 1, \ldots$, increases by one (or $2L_{rel} + 1$ if the degeneracy of the different M_L values is accounted for explicitly) as n increases by one (see Figs. 2 and 5 and Table IV). (iii) The energy spectrum corresponding to "gaslike" states has to be identical in the limits $a^{(aa)} \to 0^-$ and $a^{(aa)} \to 0^+$. (iv) It can be easily checked that (i)–(iii) are consistent with the fact that the energy $E_{rel}(2,1)$ of all but one level of each noninteracting manifold with a given L_{rel} decreases by $\hbar\omega$ when going from $a^{(aa)} \to 0^-$ to $a^{(aa)} \to \infty$ and by another $\hbar\omega$ when going from $a^{(aa)} \to \infty$ to $a^{(aa)} \to 0^+$. The dropping of the energies by $2\hbar\omega$ as $a^{(aa)}$ changes from 0^- through $\pm\infty$ to 0^+ is similar to the $2\hbar\omega$ dropping of the excited-state s-wave energies of the two-particle system (see dashed lines in Fig. 1) and can be interpreted as one pair (consisting of a spin-up atom and a spin-down atom) feeling the s-wave interaction while the other spin-up atom carries the angular momentum.

Interestingly, the observations described in the previous paragraph allow an approximate determination of the K_{unit} coefficients [see Eq. (32)]. Observation (i) implies that the lowest K_{unit} coefficient for a given L_{rel} is approximately given by $K_{unit,model} = L_{rel} + 1/2$ in the large L_{rel} limit. As discussed in Sec. II B, each K_{unit} coefficient determines the starting point of a ladder of energy levels, which are spaced by $2\hbar\omega$ and associated with an increasing number of nodes along the hyperradial coordinate R. It is evident from Figs. 5(b)–5(d) that these states, which are characterized by the same hyperangular quantum number but different hyperradial quantum numbers q, transform into atom plus dimer states in the $a^{(aa)} \to 0^+$ limit, which are characterized by the effective orbital angular momentum quantum number $l_{eff} = 0$ and different radial quantum numbers n_{eff}. Interpreting the atom-dimer distance coordinate as the hyperradial coordinate in the $a^{(aa)} \to 0^+$ limit, the identification $q \leftrightarrow n_{eff}$ suggests itself. Using observation (iv), the remaining K_{unit} coefficients at unitarity are approximately given by $K_{unit,model} = L_{rel} + 1/2 + 2n$ for $L_{rel} > 0$ and natural parity states [for each $n = 1, 2, \ldots$, the q quantum number in Eq. (32) takes the values $q = 0, 1, \ldots$]. Figure 6(a) shows that the difference between K_{unit} (symbols) and $K_{unit,model}$ (dotted lines) decreases as L_{rel} increases. The difference between K_{unit}
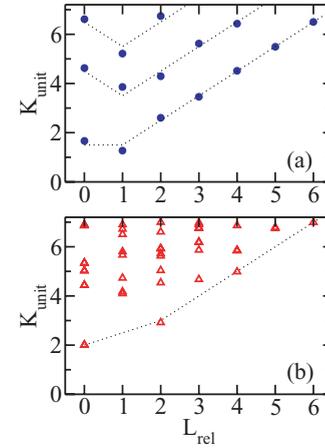
FIG. 6. (Color online) Symbols show the coefficients K_{unit} that correspond to natural parity states for (a) the three-fermion system and (b) the four-fermion system as a function of the angular momentum quantum number L_{rel}. Dotted lines show the coefficients $K_{unit,model}$ (see text for details).

and $K_{unit,model}$ has previously been quantified by Werner and Castin within a semiclassical WKB framework [32].

The $L_{rel} = 0$ spectrum is different from the $L_{rel} > 0$ spectra for two reasons. First, the effective atom-dimer system is described by an effective atom-dimer s-wave scattering length $a^{(ad)}$, which leads to a decrease of approximately $\hbar\omega$ of the energy levels belonging to the atom plus dimer family as $a^{(aa)}$ changes from ∞ to 0^+. Second, the symmetry constraint in the $a^{(aa)} \to 0^-$ limit pushes the energy of the lowest $L_{rel} = 0$ state up by $\hbar\omega$ compared to that with $L_{rel} = 1$. Dashed lines in Fig. 5(a) show the eigenenergies of the effective atom plus dimer model, i.e., the eigenenergies of Eq. (15) for $k = ad$ with $a^{(ad)}$ given by Eq. (13). It can be seen that the agreement between the energies of this effective model and a subset of the full three-fermion energies is good for small positive $a^{(aa)}$ and qualitatively correct throughout the entire crossover regime. Using the effective atom plus dimer model, the energy at unitarity of a subset of states is approximately given by $E_{rel}(2,1) \approx E_{dimer} + (2q + 5/2)\hbar\omega$, implying $K_{unit,model} = 3/2$. For comparison, the exact value is $K_{unit} = 1.666$ [32]. The other K_{unit} coefficients for $L_{rel} = 0$ can be estimated by using the fact that the energy of one subset of states drops by $\hbar\omega$ in going from $a^{(aa)} \to \infty$ to $a^{(aa)} \to 0^+$, implying $E_{unit,rel}(2,1) \approx (5/2 + 2q + 2n)\hbar\omega$ with $n = 1, 2, \ldots$ and $q = 0, 1, \ldots$. This estimate yields $K_{unit,model} = 5/2 + 2n$ for $n = 1, 2, \ldots$. Figure 6(a) shows that the $K_{unit,model}$ (dotted lines) reproduce the exact K_{unit} coefficients (symbols) fairly well.

B. Four-fermion system

This section discusses the energy spectrum of the four-fermion system throughout the BCS-BEC crossover. We primarily focus on the energies corresponding to natural parity states but also consider those states corresponding to unnatural parity. To determine the energy spectrum corresponding to states with natural parity, we use the stochastic variational approach with the basis functions given in Eq. (36); our basis set optimization treats either one state at a time or a subset of states simultaneously. For a given atom-atom scattering length $a^{(aa)}$,

we determine the energies for various ranges, $r_0 = 0.01a_{ho}$–$0.09a_{ho}$, of the two-body Gaussian interaction potential and extrapolate the finite-range energies to $r_0 \to 0$. For negative scattering lengths $a^{(aa)}$, we find that the four-fermion energies depend linearly on r_0 for all L_{rel} considered. In this regime, we typically calculate the energies for three different r_0 and then determine the $r_0 \to 0$ energies by performing a linear fit. For positive scattering lengths $a^{(aa)}$, the energetically low-lying part of the spectrum is dominated by the "internal" energy of the dimer(s) formed. As discussed in more detail below, the lowest energy family for even L_{rel} can be described by an effective two-boson model, while the lowest energy family for odd L_{rel} consists of states that can be thought of as consisting of a dimer and two atoms as $a^{(aa)} \to 0^+$ (see Sec. II and below). Correspondingly, for positive $a^{(aa)}$ and even L_{rel}, we subtract twice the dimer binding energy from the four-fermion energies for each r_0 and extrapolate the scaled four-fermion energies to the $r_0 \to 0$ limit. We typically consider five different r_0 and extract the scaled zero-range energies by performing a quadratic fit to the scaled finite-range four-fermion energies. The zero-range four-fermion energies themselves are then obtained by adding twice the zero-range dimer energy, i.e., $2E_{dimer}$. For odd L_{rel}, we subtract (and later add) the dimer energy as opposed to twice the dimer energy but proceed analogously otherwise.

The energies of a large number of energy levels corresponding to natural parity states are reported in the auxiliary materials [68] for atom-atom scattering lengths $a^{(aa)}$ ranging from 0^- over ∞ to $0.2a_{ho}$ for $L_{rel} \leqslant 4$. Here, we present comprehensive benchmark results for the four-fermion system with finite angular momentum throughout the crossover region. Tables VI and VII summarize the energies of the four-fermion system at unitarity for natural parity states with $L_{rel} = 0$ to $L_{rel} = 8$ as well as for one unnatural parity state. To our knowledge, results at unitarity for $L_{rel} > 0$ have not been presented before. We estimate that our extrapolated zero-range energies for the energetically lowest-lying $L_{rel} = 0$ state is accurate to better than 0.1% for most scattering lengths $a^{(aa)}$, including infinitely large $a^{(aa)}$. Near the avoided crossings around $a^{(aa)} \approx a_{ho}$ (see, e.g., Fig. 10), however, the accuracy decreases by up to an order of magnitude. Generally speaking, we find that the accuracy of the extrapolated zero-range energies also decreases for energetically higher lying states and for states with larger L_{rel}. The eigenenergies reported in Tables VI and VII are labeled by the hyperradial quantum number q. Following Eq. (32), we identify this quantum number by looking for $2\hbar\omega$ spacings between energy pairs. Inspection of Table VI shows that the energies with $q > 0$ lie, within our numerical accuracy, $2\hbar\omega$ above an energy with $q - 1$ (see the nearly identical K_{unit} coefficients in the fourth column of Tables VI and VII). Figure 6(b) shows the K_{unit} coefficients corresponding to natural parity states of the four-fermion system as a function of L_{rel}. Compared to the three-fermion system, the four-fermion system exhibits a notably denser energy spectrum at unitarity [see Figs. 6(a) and 6(b)].

Lines in Fig. 7 show the extrapolated zero-range energies for the four-fermion system corresponding to natural parity states with $L_{rel} = 0$ to $L_{rel} = 4$ as a function of the inverse s-wave scattering length $1/a^{(aa)}$ for negative $a^{(aa)}$. In the $a^{(aa)} \to 0^-$ limit, the three energetically lowest-lying four-fermion

TABLE VI. Extrapolated zero-range energies $E_{unit,rel}(2,2)$ for natural parity states with $L_{rel} \leqslant 4$ [$E_{unit,rel}(2,2) \leqslant 8.5\hbar\omega$]. The uncertainty of the energies is estimated to be in the last digit reported. For comparison, the lowest energy of the $(L_{rel}, \Pi_{rel}) = (1, +1)$ state is $E_{unit,rel} = 5.088(20)\hbar\omega$.

L_{rel}	Π_{rel}	q	K_{unit}	$E_{unit,rel}/E_{ho}$
0	+1	0	2.009	3.509
0	+1	1	2.010	5.510
0	+1	0	4.444	5.944
0	+1	0	5.029	6.529
0	+1	0	5.347	6.847
0	+1	2	2.017	7.517
0	+1	1	4.446	7.946
0	+1	0	6.864	8.364
0	+1	0	6.905	8.405
1	−1	0	4.098	5.598
1	−1	0	4.176	5.676
1	−1	0	4.730	6.230
1	−1	0	5.669	7.169
1	−1	0	5.807	7.307
1	−1	1	4.101	7.601
1	−1	1	4.180	7.680
1	−1	0	6.505	8.005
1	−1	0	6.724	8.224
1	−1	1	4.732	8.232
1	−1	0	6.904	8.404
2	+1	0	2.918	4.418
2	+1	0	4.539	6.039
2	+1	1	2.920	6.420
2	+1	0	5.039	6.539
2	+1	0	5.629	7.129
2	+1	0	5.722	7.222
2	+1	0	5.925	7.425
2	+1	0	5.927	7.427
2	+1	1	4.542	8.042
2	+1	0	6.707	8.207
2	+1	2	2.924	8.424
2	+1	0	7.001	8.501
3	−1	0	4.676	6.176
3	−1	0	5.871	7.371
3	−1	0	6.191	7.691
3	−1	0	6.194	7.694
3	−1	1	4.678	8.178
3	−1	0	6.764	8.264
3	−1	0	6.771	8.271
3	−1	0	6.904	8.404
3	−1	0	6.977	8.477
4	+1	0	4.985	6.485
4	+1	0	5.838	7.338
4	+1	0	5.868	7.368
4	+1	0	6.865	8.365
4	+1	1	4.984	8.484

energy manifolds around $E_{ni,rel}(2,2) = 13\hbar\omega/2$, $15\hbar\omega/2$, and $17\hbar\omega/2$ consist of two, four, and 15 states, respectively (here, the $2L_{rel} + 1$ degeneracy due to the M_L quantum number is not included in counting the states; see also Table V). For comparison, pluses in Fig. 7 show the energetically lowest-lying unnatural parity state with $(L_{rel}, \Pi_{rel}) = (1, +1)$; in this

TABLE VII. Lowest two extrapolated zero-range energies $E_{\text{unit,rel}}(2,2)$ for the four-fermion system with natural parity and $L_{\text{rel}} = 5\text{--}8$ at unitarity. The uncertainty of the extrapolated zero-range energies is estimated to be in the last or second to last digit reported.

L_{rel}	Π_{rel}	q	K_{unit}	$E_{\text{unit,rel}}/E_{\text{ho}}$
5	-1	0	6.745	8.245
5	-1	0	6.790	8.290
6	$+1$	0	6.996	8.496
6	$+1$	0	7.781	9.281
7	-1	0	8.769	10.269
7	-1	0	8.777	10.277
8	$+1$	0	8.998	10.498
8	$+1$	0	9.775	11.275

case, the energies are calculated for a Gaussian two-body potential with small but finite r_0 and have not been extrapolated to the $r_0 \to 0$ limit. Figure 7 shows that the three energy manifolds remain distinguishable up to $a_{\text{ho}}/a^{(aa)} \approx -2$ but start to overlap notably in the strongly interacting regime.

We now discuss the weakly attractive regime of the four-fermion energy spectrum in more detail. The coefficients $c^{(1)}$ that determine the perturbative energy shifts $E^{(1)}$ are summarized in the last column of Table V for the first three energy manifolds with $E_{\text{ni,rel}} = 13\hbar\omega/2$, $15\hbar\omega/2$, and $17\hbar\omega/2$. Figure 8 compares the four-fermion spectrum near $E_{\text{rel}}(2,2) \approx 13/2\hbar\omega$ calculated by the stochastic variational approach [squares, diamonds, and pluses show the energy levels corresponding to states with $(L_{\text{rel}}, \Pi_{\text{rel}}) = (0,+1)$, $(2,+1)$, and $(1,+1)$, respectively] with that calculated perturbatively (solid and dashed lines show the energies corresponding to states with natural and unnatural parity, respectively). As expected, the agreement is excellent for small $|a^{(aa)}|$ and worsens with increasing $|a^{(aa)}|$. For small $|a^{(aa)}|$, the energy level with unnatural parity is affected less strongly by the two-body interactions than the energy levels with natural parity. Inspection of Table V shows that this is a general trend; i.e., within a given manifold, the energy level shifted most strongly is that corresponding to the natural parity state with the smallest allowed angular momentum.
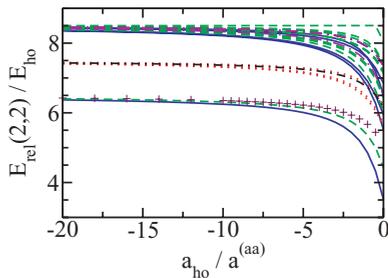
FIG. 7. (Color online) Four-fermion energies $E_{\text{rel}}(2,2)$ as a function of the inverse s-wave scattering length $a_{\text{ho}}/a^{(aa)}$ with $1/a^{(aa)} \leqslant 0$. For $a^{(aa)} \to 0^-$, all energy levels corresponding to natural parity states around $E_{\text{ni,rel}} = 13\hbar\omega/2$, $15\hbar\omega/2$, and $17\hbar\omega/2$ are shown. Solid, dotted, dashed, dash-dotted, and dash-dash-dotted lines show the zero-range energies corresponding to natural parity states with $L_{\text{rel}} = 0$ to $L_{\text{rel}} = 4$. Pluses show the energy of the energetically lowest-lying unnatural parity state with $L_{\text{rel}} = 1$.
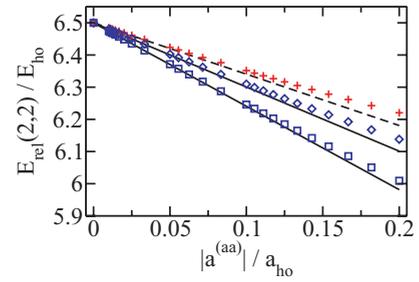
FIG. 8. (Color online) Four-fermion energies $E_{\text{rel}}(2,2)$ as a function of the absolute value of the s-wave scattering length $|a^{(aa)}|$ for small $|a^{(aa)}|$, $a^{(aa)} \leqslant 0$, and $E_{\text{rel}}(2,2) \approx 13\hbar\omega/2$. Squares, diamonds, and pluses show the numerically determined four-fermion energies for $(L_{\text{rel}}, \Pi_{\text{rel}}) = (0,+1)$, $(L_{\text{rel}}, \Pi_{\text{rel}}) = (2,+1)$, and $(L_{\text{rel}}, \Pi_{\text{rel}}) = (1,+1)$, respectively. Solid and dashed lines show the perturbative results for natural and unnatural parity states, respectively.

To illustrate the behavior of the energy spectrum for a higher energy manifold, Fig. 9 shows the energies corresponding to the eight states with $(L_{\text{rel}}, \Pi_{\text{rel}}) = (2,+1)$ around $E_{\text{rel}} \approx 17\hbar\omega/2$. Again, the agreement between the numerically determined energies (diamonds) and the perturbatively determined energies (solid lines) is excellent for small $|a^{(aa)}|$. Interestingly, within the perturbative treatment, one of the $(L_{\text{rel}}, \Pi_{\text{rel}}) = (2,+1)$ states is not affected by the s-wave interactions, implying that the wave function vanishes whenever two unlike fermions approach each other closely. It turns out that the perturbative result in this case is exact, i.e., there exists a $(L_{\text{rel}}, \Pi_{\text{rel}}) = (2,+1)$ state with energy $E_{\text{rel}}(2,2) = 17\hbar\omega/2$ for all scattering lengths $a^{(aa)}$.

Figures 4(c) and 4(d) show the distributions of the $c^{(1)}$ coefficients for the fourth and fifth energy manifolds with $E_{\text{rel}}(2,2) \approx 19\hbar\omega/2$ and $E_{\text{rel}}(2,2) \approx 21\hbar\omega/2$, respectively. Compared to the three-particle case [Figs. 4(a) and 4(b)], the degeneracies increase more rapidly, as can be seen by the higher frequency with which the $c^{(1)}$ coefficients occur. Furthermore, the $c^{(1)} = 0$ bin no longer dominates the distribution, since both natural and unnatural parity states are effected by the zero-range interactions.

Next, we discuss the energy spectrum in the strongly interacting regime and in the $a^{(aa)} \to 0^+$ limit. For small $a^{(aa)}$,
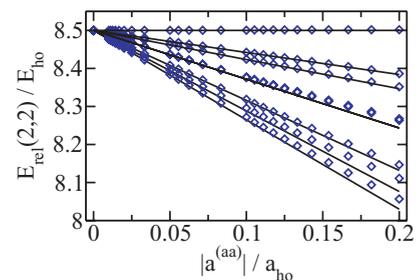
FIG. 9. (Color online) Four-fermion energies $E_{\text{rel}}(2,2)$ as a function of the absolute value of the s-wave scattering length $|a^{(aa)}|$ for small $|a^{(aa)}|$ ($a^{(aa)} \leqslant 0$), $E_{\text{rel}}(2,2) \approx 17\hbar\omega/2$ and $(L_{\text{rel}}, \Pi_{\text{rel}}) = (2,+1)$. Diamonds show the numerically determined four-fermion energies, while solid lines show the perturbative results. Note that the fourth and fifth states (counted from the bottom) are nearly degenerate for the scattering length range depicted.

FIG. 11. (Color online) Symbols show the difference between the lowest coefficient K_{unit} obtained from our numerically determined four-fermion energies and the lowest coefficient $K_{unit,model}$ predicted by the simple dimer-dimer model discussed in the text as a function of L_{rel} (L_{rel} even). To guide the eye symbols are connected by dotted lines.

FIG. 10. (Color online) Scaled four-fermion energies $E_{rel}(2,2) - 2E_{dimer}$ as a function of $a_{ho}/a^{(aa)}$ for (a) $(L_{rel}, \Pi_{rel}) = (0, +1)$, (b) $(L_{rel}, \Pi_{rel}) = (2, +1)$, and (c) $(L_{rel}, \Pi_{rel}) = (4, +1)$. Symbols show the numerically determined energies, while dashed lines show the energies predicted by the effective dimer-dimer model (see text for details).

the energetically lowest-lying states with even L_{rel} belong to the "dimer plus dimer" family, while the energetically lowest-lying states with odd L_{rel} belong to the "dimer plus atom plus atom" family. Motivated by this observation (see also Refs. [35,40,67]) and by our discussion of the three-fermion system (see Sec. III A), Figs. 10(a), 10(b), and 10(c) show the scaled energies $E_{rel}(2,2) - 2E_{dimer}$ for $L_{rel} = 0$, 2, and 4, respectively. The scaled four-fermion spectra for $L_{rel} = 2$ and 4 contain a set of nearly constant scaled energies given by $E_{rel}(2,2) - 2E_{dimer} \approx (3/2 + L_{rel} + 2q)\hbar\omega$, where $q = 0, 1, \ldots$ [see dashed lines in Figs. 10(b) and 10(c)]. Figures 10(b) and 10(c) show that this description improves with increasing L_{rel}. The set of constant scaled energies $E_{rel}(2,2) - 2E_{dimer}$ is predicted to exist within the effective two-boson model, which treats the composite bosons as noninteracting if $L_{rel} > 0$ and L_{rel} even [see the discussion below Eq. (15) in Sec. II]. Using that a subset of the scaled energies is approximately constant and that the dimer energy E_{dimer} equals $\hbar\omega/2$ at unitarity, the lowest K_{unit} coefficient is, for L_{rel} even and $L_{rel} > 0$, approximately given by $K_{unit,model} = L_{rel} + 1$. The energy levels associated with these K_{unit} coefficients have the minimally allowed number of excitations in the hyperangular degrees of freedom and q excitations along the hyperradial coordinate R; these states transform, as $a^{(aa)}$ changes from ∞ to 0^+, to "dimer plus dimer" states with n_{eff} radial excitations. Since the dimers are

composite bosons, an analogous set of states does not exist for odd L_{rel}. Squares in Fig. 11 show the difference between the lowest K_{unit} coefficient and the $K_{unit,model}$, where K_{unit} is taken from Tables VI and VII for $L_{rel} = 2$–8 and L_{rel} even. This figure supports our conjecture that the lowest coefficient K_{unit} converges to the value $K_{unit,model}$ in the large L_{rel} limit.

The behavior of the scaled energies for $L_{rel} = 0$ is different from that of the scaled energies for $L_{rel} > 0$ (L_{rel} even). Figure 10(a) does not show a set of nearly constant scaled energy levels but instead shows a set of scaled energies that drop by approximately $\hbar\omega$ in going from $a^{(aa)} \to 0^-$ to $a^{(aa)} = \infty$ and by another $\hbar\omega$ in going from $a^{(aa)} = \infty$ to $a^{(aa)} \to 0^+$. Dashed lines in Fig. 10 show the energies predicted by the effective dimer-dimer model. To obtain these energies, we solve Eq. (15) for $k = dd$ and use Eq. (14) to express the effective dimer-dimer scattering length $a^{(dd)}$ in terms of the atom-atom scattering length $a^{(aa)}$ throughout the entire crossover. The dashed lines agree surprisingly well with the full four-fermion energies throughout the entire crossover. Comparison with Fig. 5(a) shows that the effective two-particle model provides a better description of the four-fermion than of the three-fermion system, particularly for negative $a^{(aa)}$. Intuitively, this might be explained by the fact that the three-fermion system contains an unpaired atom while all atoms participate in the molecule formation in the four-fermion system. Figure 10 suggests that the four-fermion energy spectrum can be interpreted by considering avoided crossings between dimer-dimer states and states that belong to the "dimer plus atom plus atom" and the "gaslike state" families. An analysis along these lines has been performed in Refs. [40,67]; however, to the best of our knowledge this type of analysis has not been previously applied to estimate the value of the lowest K_{unit} coefficient for $L_{rel} = 0$. Using that the energy in the $a^{(aa)} \to 0^+$ limit is given by $2E_{dimer} + (3/2 + 2n_{eff})\hbar\omega$ and that the energy at unitarity is—using the argument above—$2E_{dimer} + (5/2 + 2q)\hbar\omega$, the lowest K_{unit} coefficient for $L_{rel} = 0$ can be estimated to be $K_{unit,model} = 2$. Table VI shows that this model is surprisingly accurate, i.e., $K_{unit} = 2.009$ (see also Fig. 11).

We find numerically that the second-lowest K_{unit} coefficient for even L_{rel} ($\Pi_{rel} = +1$) and the lowest K_{unit} coefficient for odd L_{rel} ($\Pi_{rel} = -1$) appear to approach $L_{rel} + 7/4$ for large L_{rel}. At present, we have no explanation for this observation.

While our analysis presented above allows the prediction of the lowest K_{unit} coefficient for all even L_{rel}, the remaining coefficients at unitarity appear to be the result of an intricate interplay of how to best distribute the angular momentum among the six interparticle distances.

IV. SUMMARY

This paper considered s-wave interacting three- and four-fermion systems under external spherically symmetric harmonic confinement. If the range r_0 of the underlying interaction potential is much smaller than the other length scales of the system, i.e., the atom-atom s-wave scattering length $a^{(aa)}$ and the harmonic oscillator length a_{ho}, then the physics of two-component equal-mass Fermi systems is universal. If the s-wave scattering length is tuned in the vicinity of a so-called broad Feshbach resonance [55,69,70], then the low-energy properties of these few-fermion systems are expected to behave universally, i.e., independently of the details of the underlying interaction potential. Our results are expected to apply to the most frequently experimentally studied species ^{6}Li and ^{40}K [22,71–76].

We have numerically determined the zero-range energy spectrum of the three- and four-fermion systems for a wide range of s-wave scattering lengths $a^{(aa)}$. Our study of the three-fermion system is based on the Lippmann-Schwinger equation, which reduces the problem to solving a set of coupled equations for each angular momentum L_{rel} [33]. The three-fermion spectrum is analyzed and interpreted following a number of different approaches. In the weakly interacting regime, the interactions are treated as a perturbation to the noninteracting trapped atomic Fermi gas. This approach correctly describes the gaslike states of the system for small $|a^{(aa)}|$, with $a^{(aa)}$ positive and negative, but does not describe states that are associated with the formation of diatomic molecules. The energies of this family of states are described by an effective two-particle Hamiltonian that treats the diatomic molecule as a composite point particle and assumes that the spare atom and the molecule interact through the s-wave scattering channel characterized by the effective atom-dimer scattering length $a^{(ad)}$. Somewhat surprisingly, this effective two-particle model describes correctly the energies of a subset of states not only quantitatively in the weakly repulsive regime but also qualitatively for negative $a^{(aa)}$ (see dashed lines in Fig. 5). Building on this observation, we developed a simple model which predicts the K_{unit} coefficients with reasonably good accuracy. In doing so, our motivation was to develop a physical picture of the general features of the three-fermion energy spectrum that can, at least partially, be generalized to larger systems. A key result of our analysis is that the energy levels determined by the lowest K_{unit} coefficient for each L_{rel} transform to "atom plus dimer" states as $a^{(aa)}$ changes from ∞ to 0^+. This "transformation" of the states can be

interpreted nicely within the hyperspherical framework. Using hyperspherical coordinates, the states for $a^{(aa)} = \infty$ and 0^+ are separable, and the widths of the avoided crossings of the energy levels for finite $a^{(aa)}$ are determined by the couplings between different hyperradial potential curves (see, e.g., Refs. [45,77–79] as well as Ref. [67]).

We also solved the time-independent Schrödinger equation for the four-fermion system for a Gaussian two-body potential with varying range r_0 using the stochastic variational approach. The resulting finite-range energies were then extrapolated to the $r_0 \to 0$ limit. The energy spectrum of the four-fermion system is much denser than that of the three-fermion system. Unlike for the three-fermion system, natural and unnatural parity states of the four-fermion system are shifted by the zero-range interactions. Our primary focus in this paper has been to characterize the energies of the lowest few states with natural parity throughout the crossover, including the infinitely strongly interacting unitary regime. As in the three-fermion case, our semianalytical perturbative approach, which utilizes hyperspherical coordinates, reproduces the numerically determined four-fermion energies with good accuracy in the weakly attractive and weakly repulsive regimes. We paid special attention to the infinitely strongly interacting regime and analyzed the energy spectrum at unitarity within an effective two-boson model. This analysis provides a physical picture of how the lowest K_{unit} coefficient for natural parity states and even L_{rel} comes about and how the associated ladder of states transforms to "dimer plus dimer" states as $a^{(aa)} \to 0^+$. Furthermore, the fact that the effective two-boson model reproduces a subset of energy levels semiquantitatively throughout the entire crossover regime suggests that the concept of the effective dimer-dimer scattering length $a^{(dd)}$ extends beyond the small $a^{(aa)}$ regime ($a^{(aa)} > 0$).

One motivation for studying small few-fermion systems is to develop a "bottom-up approach" that investigates the microscopic physics of two-component Fermi gases by treating successively larger systems. With this motivation in mind, the three-fermion system can be considered the smallest system that models spin-imbalanced Fermi gases [33], while the four-fermion system can be considered the smallest system that models pairing physics throughout the BCS-BEC crossover of spin-balanced Fermi gases [40]. In the future, it will be interesting to extend the studies presented here to larger equal-mass few-fermion systems as well as to unequal-mass fermionic and bosonic systems. We also hope to use the perturbative treatment of the four-fermion system to estimate the fourth-order virial coefficient in the weakly interacting regimes.

ACKNOWLEDGMENTS

---

[1] L. Platter, H. W. Hammer, and Ulf-G. Meissner, Phys. Rev. A **70**, 052101 (2004).

[2] M. T. Yamashita, L. Tomio, A. Delfino, and T. Frederico, Europhys. Lett. **75**, 555 (2006).

[3] G. J. Hanna and D. Blume, Phys. Rev. A **74**, 063604 (2006).

[4] H. W. Hammer and L. Platter, Eur. Phys. J. A **32**, 113 (2007).

[5] J. von Stecher, J. P. D'Incao, and C. H. Greene, Nature Phys. **5**, 417 (2009).

[6] Y. J. Wang and B. D. Esry, Phys. Rev. Lett. **102**, 133201 (2009).

[7] F. Ferlaino, S. Knoop, M. Berninger, W. Harm, J. P. D'Incao, H.-C. Nägerl, and R. Grimm, Phys. Rev. Lett. **102**, 140401 (2009).

[8] M. Zaccanti, B. Deissler, C. D'Errico, M. Fattori, M. Jona-Lasinio, S. Müller, G. Roati, M. Inguscio, and G. Modugno, Nature Phys. **5**, 586 (2009).

[9] S. E. Pollack, D. Dries, and R. G. Hulet, Science **326**, 1683 (2009).

[10] E. Braaten and H.-W. Hammer, Phys. Rep. **428**, 259 (2006).

[11] G. A. Baker Jr., Phys. Rev. C **60**, 054311 (1999).

[12] K. M. O'Hara, S. L. Hemmer, M. E. Gehm, S. R. Granade, and J. E. Thomas, Science **298**, 2179 (2002).

[13] T.-L. Ho, Phys. Rev. Lett. **92**, 090402 (2004).

[14] S. Tan, e-print arXiv:cond-mat/0412764v2.

[15] S. Y. Chang and V. R. Pandharipande, Phys. Rev. Lett. **95**, 080402 (2005).

[16] G. E. Astrakharchik, J. Boronat, J. D. Casulleras, and S. Giorgini, Phys. Rev. Lett. **93**, 200404 (2004).

[17] S. Y. Chang, V. R. Pandharipande, J. Carlson, and K. E. Schmidt, Phys. Rev. A **70**, 043602 (2004).

[18] J. E. Thomas, J. Kinast, and A. Turlapov, Phys. Rev. Lett. **95**, 120402 (2005).

[19] Y. Castin, C. R. Phys. **5**, 407 (2004).

[20] F. Werner and Y. Castin, Phys. Rev. A **74**, 053604 (2006).

[21] D. T. Son and M. Wingate, Ann. Phys. (NY) **321**, 197 (2006).

[22] J. T. Stewart, J. P. Gaebler, C. A. Regal, and D. S. Jin, Phys. Rev. Lett. **97**, 220406 (2006).

[23] S. Tan, Ann. Phys. (NY) **323**, 2952 (2008).

[24] S. Tan, Ann. Phys. (NY) **323**, 2971 (2008).

[25] S. Tan, Ann. Phys. (NY) **323**, 2987 (2008).

[26] E. Braaten and L. Platter, Phys. Rev. Lett. **100**, 205301 (2008).

[27] E. Braaten, D. Kang, and L. Platter, Phys. Rev. A **78**, 053606 (2008).

[28] F. Werner and Y. Castin, e-print arXiv:1001.0774 [cond-mat].

[29] M. Greiner, O. Mandel, T. Esslinger, T. W. Hänsch, and I. Bloch, Nature (London) **415**, 39 (2002).

[30] M. Köhl, H. Moritz, T. Stöferle, K. Günter, and T. Esslinger, Phys. Rev. Lett. **94**, 080403 (2005).

[31] G. Thalhammer, K. Winkler, F. Lang, S. Schmid, R. Grimm, and J. H. Denschlag, Phys. Rev. Lett. **96**, 050402 (2006).

[32] F. Werner and Y. Castin, Phys. Rev. Lett. **97**, 150401 (2006).

[33] J. P. Kestner and L. M. Duan, Phys. Rev. A **76**, 033611 (2007).

[34] I. Stetcu, B. R. Barrett, U. van Kolck, and J. P. Vary, Phys. Rev. A **76**, 063613 (2007).

[35] J. von Stecher, C. H. Greene, and D. Blume, Phys. Rev. A **77**, 043619 (2008).

[36] K. Varga and Y. Suzuki, Phys. Rev. C **52**, 2885 (1995).

[37] K. Varga, P. Navratil, J. Usukura, and Y. Suzuki, Phys. Rev. B **63**, 205308 (2001).

[38] Y. Suzuki and K. Varga, *Stochastic Variational Approach to Quantum Mechanical Few-Body Problems* (Springer-Verlag, Berlin, 1998).

[39] H. H. B. Sørensen, D. V. Fedorov, and A. S. Jensen, AIP Conf. Proc. **777**, 12 (2005).

[40] J. von Stecher and C. H. Greene, Phys. Rev. Lett. **99**, 090402 (2007).

[41] J. von Stecher, C. H. Greene, and D. Blume, Phys. Rev. A **76**, 053613 (2007).

[42] D. Blume, J. von Stecher, and C. H. Greene, Phys. Rev. Lett. **99**, 233201 (2007).

[43] D. Blume and K. M. Daily, Phys. Rev. A **80**, 053626 (2009).

[44] J. Avery, *Hyperspherical Harmonics: Applications in Quantum Theory* (Kluwer Academic, Dordrecht, 1989).

[45] C. D. Lin, Phys. Rep. **257**, 1 (1995).

[46] J. L. Bohn, B. D. Esry, and C. H. Greene, Phys. Rev. A **58**, 584 (1998).

[47] N. K. Timofeyuk, Phys. Rev. C **65**, 064306 (2002).

[48] N. K. Timofeyuk, Phys. Rev. C **69**, 034336 (2004).

[49] M. F. de la Ripelle, S. A. Sofianos, and R. M. Adam, Ann. Phys. (NY) **316**, 107 (2005).

[50] S. T. Rittenhouse, M. J. Cavagnero, J. von Stecher, and C. H. Greene, Phys. Rev. A **74**, 053624 (2006).

[51] U. Fano, D. Green, J. L. Bohn, and T. A. Heim, J. Phys. B **32**, R1 (1999).

[52] S. T. Rittenhouse and C. H. Greene, J. Phys. B **41**, 205302 (2008).

[53] E. Fermi, Nuovo Cimento **11**, 157 (1934).

[54] D. S. Petrov, C. Salomon, and G. V. Shlyapnikov, Phys. Rev. Lett. **93**, 090404 (2004).

[55] D. S. Petrov, C. Salomon, and G. V. Shlyapnikov, J. Phys. B **38**, S645 (2005).

[56] D. S. Petrov, Phys. Rev. A **67**, 010703(R) (2003).

[57] K. Huang and C. N. Yang, Phys. Rev. **105**, 767 (1957).

[58] G. V. Skorniakov and K. A. Ter-Martirosian, Zh. Eksp. Teor. Fiz. **31**, 775 (1956) [Sov. Phys. JETP **4**, 648 (1957)].

[59] C. Mora, R. Egger, A. O. Gogolin, and A. Komnik, Phys. Rev. Lett. **93**, 170403 (2004).

[60] C. Mora, R. Egger, and A. O. Gogolin, Phys. Rev. A **71**, 052705 (2005).

[61] T. Busch, B.-G. Englert, K. Rzążewski, and M. Wilkens, Found. Phys. **28**, 549 (1998).

[62] V. Efimov, Yad. Fiz. **12**, 1080 (1970) [Sov. J. Nucl. Phys. **12**, 598 (1971)].

[63] V. N. Efimov, Nucl. Phys. A **210**, 157 (1973).

[64] J. P. D'Incao and B. D. Esry, Phys. Rev. Lett. **94**, 213201 (2005).

[65] J. von Stecher and C. H. Greene, Phys. Rev. A **80**, 022504 (2009).

[66] X.-J. Liu, H. Hu, and P. D. Drummond, Phys. Rev. Lett. **102**, 160401 (2009).

[67] J. von Stecher, Ph.D. thesis, University of Colorado, Boulder, 2008; available at [http://jila.colorado.edu/pubs/thesis/].

[68] See supplementary material at [http://link.aps.org/supplemental/10.1103/PhysRevA.81.053615].

[69] S. Giorgini, L. P. Pitaevskii, and S. Stringari, Rev. Mod. Phys. **80**, 1215 (2008).

[70] R. B. Diener and T.-L. Ho, e-print arXiv:cond-mat/0405174.

[71] B. DeMarco and D. S. Jin, Science **285**, 1703 (1999).

[72] M. Greiner, C. A. Regal, and D. S. Jin, Nature (London) **426**, 537 (2003).

[73] M. W. Zwierlein, C. A. Stan, C. H. Schunck, S. M. F. Raupach, S. Gupta, Z. Hadzibabic, and W. Ketterle, Phys. Rev. Lett. **91**, 250401 (2003).

[74] T. Bourdel, J. Cubizolles, L. Khaykovich, K. M. F. Magalhaes, S. J. J. M. F. Kokkelmans, G. V. Shlyapnikov, and C. Salomon, Phys. Rev. Lett. **91**, 020402 (2003).

[75] K. E. Strecker, G. B. Partridge, and R. G. Hulet, Phys. Rev. Lett. **91**, 080406 (2003).

[76] J. Kinast, S. L. Hemmer, M. E. Gehm, A. Turlapov, and J. E. Thomas, Phys. Rev. Lett. **92**, 150402 (2004).

[77] L. M. Delves, Nucl. Phys. **9**, 391 (1958).

[78] L. M. Delves, Nucl. Phys. **20**, 275 (1960).

[79] J. Macek, J. Phys. B **1**, 831 (1968).